Deep uncertainty quantification: with an application to integrated assessment models*

Preliminary and incomplete: do not share without the consent of the authors

Felix Kübler[†], Aleksandra Friedl[‡], Simon Scheidegger[§], Takafumi Usui[¶]

August 20, 2023

Abstract

This paper presents a comprehensive method to efficiently solve non-stationary, nonlinear, stochastic integrated assessment models (IAMs) and perform parametric uncertainty quantification. Our approach comprises two main components: a deep learning-based algorithm to solve IAMs globally as a function of endogenous, exogenous, as well as uncertain parameters in a single model evaluation. Secondly, we devise a Gaussian process-based surrogate model to analyze quantities of interest, such as the social cost of carbon, in relation to model input parameters, facilitating streamlined estimation of Sobol' indices, Shapley values, and univariate effects. To demonstrate our method's efficacy, we introduce a high-dimensional stochastic IAM, aligned with cutting-edge climate science. This model incorporates a social planner with recursive preferences, iterative belief updates of equilibrium climate sensitivity via Bayes' rule, and stochastic climate tipping. Uncertainty quantification results reveal a decreasing uncertainty in equilibrium climate sensitivity over time, while the intertemporal elasticity of substitution predominantly influences the social cost of carbon by 2100.

Keywords: Climate policy, Epstein-Zin preferences, Climate tipping, Deep learning, Uncertainty quantification, Gaussian processes
JEL classification: C61, C63, D58, H23, Q54, Q58

*We thank Lars Hansen, Alena Miftakhova, Karl Schmedders, Christian Traeger, Frank Venmans, as well as seminar and conference participants at the University of Chicago, the University of Lausanne, Imperial College, ESSEC, CERGE-EI Prag, ARIC Hamburg, the University of Geneva, the University of Hamburg, the University of Colorado Boulder, the University of Pennsylvania, the Australian National University, and SAET 2023 for helpful comments and suggestions. This work was generously supported by the Swiss National Science Foundation (SNF), under project ID "Can Economic Policy Mitigate Climate-Change".

[†]Department for Banking and Finance, University of Zürich, Switzerland, and SFI. Email: felix.kuebler@bf.uzh.ch

[‡]Department of Economics, HEC Lausanne, University of Lausanne. Switzerland. Email: aleksandra.malova@unil.ch

[§]Department of Economics, HEC Lausanne, University of Lausanne, Switzerland; Enterprise for Society (E4S). Email: simon.scheidegger@unil.ch

[¶]Department for Banking and Finance, University of Zürich, Switzerland. Email: takafumi.usui@bf.uzh.ch

1 Introduction

Integrated assessment models (IAMs) serve as a pivotal instrument for quantifying the prospective repercussions of anthropogenic climate change on mankind. These models are instrumental in facilitating well-informed policy deliberations and in the prudent management of associated risks. Nevertheless, akin to the case with all economic models, the ramifications they convey could occasionally exhibit considerable reliance on assumptions (which at times can be limiting) pertaining to the parameters and functional configurations embraced by the modeler. In light of this limitation, Pindyck (2013, p.860) issued a cautionary note regarding the broad application of IAMs, asserting that these models possess "*...have crucial flaws that make them close to useless as tools for policy analysis.*".

Rather than perceiving uncertainty as an insurmountable constraint on the applicability of this entire category of models, we embrace it by introducing a comprehensive framework for uncertainty quantification (UQ) within IAMs in this study. Our approach unfolds in two parts: First, we present a stochastic IAM integrated with Bayesian learning concerning the equilibrium climate sensitivity (ECS), aiming to capture the most prominent wellspring of uncertainty inherent in IAMs. Second, we devise a versatile and highly efficient computational technique named "Deep Uncertainty Quantification" (Deep UQ) to compute global solutions[1] and perform parametric UQ particularly suitable for addressing the challenges posed by high-dimensional, stochastic, non-stationary, and nonlinear model typologies.

We present a novel model that encompasses a comprehensive array of key components of IAMs. To our knowledge, these components have not been collectively investigated in quantitative work due to the computational limitations of existing methods. Moreover, they have not been examined through the lens of UQ to study various quantities of interest. These include the sensitivity of the social cost of carbon (SCC)[2]

[1] We adopt the nomenclature from Brumm and Scheidegger (2017), referring to a "global solution" as a solution computed utilizing equilibrium conditions at numerous points within the state space of a dynamic model, as opposed to a "local solution" which relies on a local approximation around a model's steady state, as achieved through perturbation methods. We employ the term "global solution method" for techniques that compute such global solutions. This utilization of "global" should not be conflated with its application in the phrase "global optimization method".

[2] The SCC can be computed as the marginal cost of carbon emissions, which is the sum of all future

concerning different types of uncertainty and the temporal evolution of its distribution. Our model is built upon the influential DICE model (Nordhaus, 2017). However, we depart from it along several significant dimensions. First, we align with recent advances in climate change economics by employing Epstein-Zin preferences (e.g., Epstein and Zin, 1989, Jensen and Traeger, 2014, Cai and Lontzek, 2019). Second, the climate module is designed in accordance with Folini et al. (2023) to ensure congruence with state-of-the-art climate science. One of the most iconic uncertainties in climate science is the ECS (Knutti et al., 2017). The ECS denotes the projected long-term temperature rise (equilibrium global mean near-surface air temperature) resulting from a doubling of atmospheric CO_2 concentration. The ECS is notoriously characterized by substantial uncertainty and fat-tailed probability distributions, potentially leading to catastrophic economic outcomes (Allen and Frame, 2007, Roe and Baker, 2007, Zaliapin and Ghil, 2010). Third, we incorporate insights from climate science literature (Roe and Baker, 2007) within our IAM framework and posit that the model's social planner can iteratively update her beliefs regarding ECS using Bayes' rule. This innovation enables us to demonstrate the planner's capacity to progressively diminish uncertainty surrounding the ECS over time. Forth, to capture the detrimental economic implications of a planet warmed by anthropogenic climate change, we adopt the damage function introduced by Weitzman (2012). Furthermore, we enrich this function by incorporating a stochastic tipping element according to Kotlikoff et al. (2021) to account for the irreversibility inherent in climate change (Lenton et al., 2008).

To tackle the aforementioned IAM numerically, we introduce Deep UQ: a method that can effectively solve non-stationary high-dimensional dynamic stochastic climate economy models and perform UQ (Saltelli et al., 2007) at negligible computational costs. An important task in UQ, and the one we are concerned with in this paper, is to measure the relative importance of the various parameter inputs to quantities of interest, such as the SCC. Importance can be quantified via the effects of changing those inputs at random. This leads to a global sensitivity analysis (GSA; see, e.g., Saltelli et al. (2007)), in which statistical methods based on an analysis of variance decomposition measure

damages resulting from an infinitesimal extra emission of CO_2 into the atmosphere, discounted at the market interest rate.

variable importance. However, the measures traditionally used in the literature, that is, Sobol' indices, univariate effects, and Shapley values (see, e.g., Owen (2014), Song et al. (2016), and references therein) typically require thousands, if not tens of thousands of model solutions to obtain convergent statistics (Harenberg et al., 2019). Thus, such an approach is a significant roadblock for performing UQ on stochastic IAMs, where a single model solution can take more than 100k CPU hours (Cai and Lontzek, 2019). Consequently, the previous literature on UQ in IAMs has typically been limited to local perturbations of solutions to stochastic models or to GSA in non-stochastic settings (see, e.g., Anderson et al. (2014), Butler et al. (2014), Miftakhova (2021), and references therein).

Our proposed numerical solution framework for performing GSA in IAMs to alleviate the abovementioned challenges consists of two distinct parts. First, we adopt and enhance a generic, deep learning-based algorithm (Azinovic et al., 2022) such that it can be used to solve stochastic IAMs globally as a function of the endogenous and exogenous state variables as well as their parameters at once in a single model solution (cf. Section 3.4). Such a "deep surrogate" – a high-precision approximation of an IAM based on deep neural networks,[3] speeds up the model evaluations required to perform UQ by orders of magnitudes and thus allows for various compute-intensive applications, as the respective tasks now simplify to interpolation tasks on the pre-computed optimal policies–which are now functions of the state variables and parameters–rather than solving an entire model for a fixed set of parameters.[4] Next, we propose constructing a second, cheap-to-evaluate surrogate model for the quantities of interests (QoIs), such as SCC, to perform GSA by using the former neural network surrogate of the IAM as an input. For computational tractability, we propose to use Gaussian

[3] For a thorough introduction to deep surrogates in economics and finance, see, e.g., Chen et al. (2021), and references therein.

[4] There are substantial computational bottlenecks in solving the type of IAMs described before as a function of endogenous and exogenous states as well as parameters in a single model evaluation globally because of i) the presence of random shocks, ii) a high-dimensional state space, iii) strong non-linearities in the optimal policies (introduced, for instance, by the presence of highly non-linear damage functions (see, e.g., Cai and Lontzek (2019), and references therein), iv) irregular, that is, non-hypercubic geometries of the set of states visited along a simulation, and v) non-stationarity. In the presence of these five features, the curse of dimensionality (Bellman, 1961) imposes a considerable roadblock. While some methods can handle a subset of i) - v), most fail at matching all five requirements. Currently, and to the best of our knowledge, the only numerically tractable method that jointly addresses all five features relies on deep neural networks.

processes (GPs; see, e.g., Renner and Scheidegger (2018), and references therein) as the surrogate modeling technique to approximate QoIs as a function of the model parameters.[5]

The remainder of this article is organized as follows. In Section 2, we provide a brief review of the related literature. In Section 3, we posit a the stochastic IAM with Bayesian learning about the ECS. Section 4 introduces our generic Deep UQ framework, and discusses its computational advantages relative to other existing methods. Section 5 presents our numerical experiments and results. Section 6 finally concludes.

2 Literature review

This paper is related to four key strands of the literature: i) research focusing on stochastic IAMs, ii) studies investigating the uncertain ECS, such as through Bayesian learning, iii) parametric UQ in IAMs, and iv) global solution methods based on machine learning.[6]

First, our paper contributes to a fast-growing body of literature on endogenizing economic and climate uncertainty in the IAMs to study, among other quantities, the SCC. Various studies (see, e.g., Golosov et al. (2014), Traeger (2021)) solve stochastic IAMs analytically and offer closed-form representations of the SCC, but it comes at the expense of strong assumptions on the carbon cycle and other functional forms that enter the model. Other work that tackles IAMs with uncertainty while trying to maintain numerical tractability by introducing various assumptions consists of Traeger (2014), which implements a state-reduced and annually calibrated recursive dynamic programming version of the canonical DICE-2007 model (Nordhaus, 2008), to study uncertainty in the damage function (Crost and Traeger, 2013, 2014), to examine long-

[5] In this study, we deliberately construct the surrogate models using two different function approximators. As a rule of thumb, one should use a surrogate model based on deep neural networks when dealing with large datasets that require learning complex nonlinear relationships. For example, in the context of solving our stochastic, nonlinear IAMs, we generate billions of observations in the solution process to train our neural network. Hence, we apply neural networks. Conversely, surrogate models based on Gaussian processes (GPs are appropriate when dealing with small datasets or when interpretability is a priority over predictive accuracy. Consequently, since in our concrete case, the SCC and other QoIs are based on relatively expensive simulations based on the model solution, we apply GPs in the latter case.

[6] Hassler et al. (2016) provide an excellent general introduction and review on IAMs.

run growth risk (Jensen and Traeger, 2014), and to introduce climate tipping points (Lemoine and Traeger, 2014, 2016). Other work is based on deterministic finite-horizon models, which investigates the implications of uncertainty by Monte-Carlo sampling in the parameter space (see, e.g., Anthoff et al. (2009), Ackerman et al. (2010), Gillingham et al. (2018), Nordhaus (2018)). One of the disadvantages of this approach is that "*(...this first-order approximation to stochastic analysis does not model a decision maker's optimal response to uncertainty.*" as Jensen and Traeger (2014) point out. In a series of papers, the team of authors (Cai and Lontzek, 2019, Lontzek and Narita, 2011, Lontzek et al., 2015, Cai et al., 2015, 2016, Lontzek et al., 2016) examines the SCC under long-run growth risk and irreversible climate tipping, dropping many analytical simplifications and resorting to high-performance computing. Barnett (2023) applies an asset pricing approach to assess uncertainty related to climate change impact, and van der Ploeg (2021) take uncertainty into account, deriving the risk-adjusted discount rate. The work presented here differs from previous studies in that we introduce a deep learning-based global solution method to solve stochastic IAMs of unprecedented complexity without the need to analytically simplify IAMs in a restrictive way or to tap high-performance computing systems.

Second, our work is related to studies examining the interplay of uncertainty in the ECS, which is an almost iconic number in climate science (Knutti et al., 2017), and the economy. Kelly and Kolstad (1999), subsequently followed, for instance, by Leach (2007), Jensen and Traeger (2013), Kelly and Tan (2015), Fitzpatrick and Kelly (2017), Hwang et al. (2017), developed a dynamic stochastic IAM in a recursive formulation and considered Bayesian learning to update a posterior distribution of ECS, which is unknown to the social planner. The literature found that the social planner with Bayesian learning resolves fat-tailed uncertainty in ECS in the long run. We build on the aforementioned literature of Bayesian learning over the ECS and combine it with the disentangled Epstein-Zin preferences to capture the risk preferences and intertemporal consumption decisions.

Third, our work contributes to studies that examine parametric uncertainty in IAMs.[7] Parametric uncertainty is often evaluated by averaging over a large number of

[7] Other sources of uncertainty, which we do not pursue in this paper but have been studied in the

deterministic Monte-Carlo simulation runs, where input parameters are drawn from relevant distributions for each simulation (Nordhaus, 2008, Ackerman et al., 2010). Saltelli and D'Hombres (2010) criticize these Monte-Carlo analyses, as they follow the so-called *one-at-a-time* (OAT) principle and can be highly misleading, failing to offer reliable policy recommendations (Crost and Traeger, 2013). In our work presented in the following, we propagate and quantify the parametric uncertainty when computing the SCC using a global sensitivity analysis (GSA) method (see, e.g., Smith (2014) for a review). Anderson et al. (2014), Butler et al. (2014) are early examples where GSA is applied to the canonical DICE model based on a large number of Monte-Carlo samples. More recently, Miftakhova (2021) constructed surrogate models[8] of the deterministic DICE model using the polynomial chaos expansion method and analyzed the GSA of the SCC on various input parameters.[9] In the GSA literature, the so-called Sobol' indices are standard metrics to measure the importance of some input parameters to overall model outcome uncertainty. An alternative, important metric in the context of UQ is the Shapley value. Owen (2014) adopted the idea of the Shapley value from the literature of cooperative game theory and demonstrated that the Shapley values intuitively attribute the overall variance of the model outcome to some input variables but not necessarily to be matched to the Sobol' indices. Song et al. (2016) proposed an efficient numerical routine to avoid traversing all permutations of input variables in estimating the Shapley values, and Iooss and Prieur (2019) efficiently speed up the numerical estimation of the Shapley values by replacing the true model with a Gaussian process-based surrogate model. Scheidegger and Bilionis (2019) intrusively added the uncertain parameters as pseudo-state variables and solved the model globally for all possible realizations of the uncertain parameters in a single model

literature, include model misspecification and ambiguity (see, e.g. Barnett et al. (2020), Zhao et al. (0)). Other sources of uncertainty encompass climate tipping points (Lenton et al., 2008), the damage function, and the transition to green technology. Weitzman (2012), for instance, introduced a tipping point to the standard Nordhaus damage function, which dramatically raises damages for temperature increases beyond a given level.

[8] A surrogate model is a high-precision approximation of an otherwise expensive-to-evaluate model, such as a high-dimensional, nonlinear, and non-stationary IAM. For more details on the applications of surrogate models in economics and finance, see, e.g., Scheidegger and Bilionis (2019), Chen et al. (2021), and references therein.

[9] Harenberg et al. (2019) is the first example in economics to present GSA based on a polynomial chaos expansion of a standard real-business-cycle model.

evaluation. When expanding the number of state variables, one has to overcome the curse of dimensionality (Bellman, 1961), which the authors addressed by applying the active subspace method (see also Constantine (2015), Kubler and Scheidegger (2021), and references therein). The work presented here contributes to the literature by introducing generic machine learning-based methods that leverage recent ideas from deep neural networks, Gaussian process regression, and the idea of surrogate models method to efficiently perform GSA in large-scale IAMs. To the best of our knowledge, we are the first to study Sobol' indices, Shapley values, and univariate effects in stochastic IAMs with Bayesian learning about the ECS.

Finally, our work relates to the emerging but fast-growing literature on machine learning-based solution methods in dynamic economic models (see, e.g., Fernández-Villaverde et al. (2020), Maliar et al. (2021), Duarte (2018), Villa and Valaitis (2019), Ebrahimi Kahou et al. (2021), Renner and Scheidegger (2018)). The numerical solution to stochastic IAMs is often achieved by applying traditional grid-based value function iteration (see, e.g., Cai and Judd (2014), Cai and Lontzek (2019), and references therein). However, while highly successful in small to mid-scale models, such methods are strongly limited when the model complexity increases, and consequently, often need to resort to high-performance computers. In our work presented below, we solve IAMs by adopting the so-called "deep equilibrium net" algorithm (Azinovic et al., 2022, Folini et al., 2023) to the context of stochastic non-stationary IAMs. To the best of our knowledge, we are the first to implement a deep learning-based solution method to solve a high-dimensional and stochastic IAM with Bayesian learning about the equilibrium climate sensitivity parameter and to propagate parametric uncertainty using a Gaussian process-based surrogate model when estimating the social cost of carbon in a computationally efficient fashion, guaranteeing affordable numerical precision, as all our numerical results are computed on a laptop. This methodological contribution will enable the IAM community to tackle much richer models without the need to use hundreds of thousands of CPU hours of computing time on a supercomputer to solve a single model specification.

3 A stochastic IAM with Bayesian learning

This section posits a discrete-time stochastic IAM with Bayesian learning about uncertain equilibrium climate sensitivity. Our model combines a stochastic representative agent framework with Epstein-Zin (-Weil) preferences (Epstein and Zin, 1989, Weil, 1989), a climate emulator[10] that follows the specification of Folini et al. (2023), and stochastic tipping points modeled similarly to Kotlikoff et al. (2021).

We proceed with the following four steps: First, in Section 3.1, we provide a brief summary of the economic building blocks of the model. Second, in Section 3.2, we outline the climate externality. Third, Section 3.3 describes our approach to modeling the learning process concerning the climate equilibrium sensitivity. Finally, in Section 3.4, we present the recursive formulation of our model. In addition, a comprehensive summary of the complete model calibration is available in Appendix A.

3.1 The economic model

The economic side of our IAM is a growth model where production produces greenhouse gas emissions, and productivity is affected by the state of the climate. Following the spirit of Nordhaus (2017), we describe our economy using a Ramsey growth model in a social planner's problem. Within this economic setup, the model assumes a single and infinitely-lived representative agent.

We adopt the Epstein-Zin (-Weil) preferences (Epstein and Zin, 1989, Weil, 1989) to address the critical aspects of risk preferences and intertemporal consumption decisions in long-run climate policy discussions (see, e.g., Crost and Traeger (2013), Cai and Lontzek (2019), and references therein). The social welfare function U_t is recursively defined as follows:

$$U_t = \left[(1-\beta) \frac{(C_t/L_t)^{1-1/\psi}}{1-1/\psi} L_t + e^{-\rho} \mathbb{E}_t \left[U_{t+1}^{1-\gamma} \right]^{\frac{1-1/\psi}{1-\gamma}} \right]^{\frac{1}{1-1/\psi}}, \tag{1}$$

where time t is discrete and measured in years, C_t represents consumption, and L_t

[10] To analyze climate change mitigation strategies, economists rely on simplified climate models – so-called climate emulators – that provide a realistic quantitative link between CO_2 emissions and global warming at low computational costs.

denotes an exogenous population path adopted from Nordhaus (2017). Furthermore, ρ denotes the pure rate of time preference, ψ measures the intertemporal elasticity of substitution, γ represents the Arrow-Pratt risk aversion parameter, and $\mathbb{E}_t[\cdot]$ denotes the expectation operator conditional on time t.

The gross output Y_t^{Gross} in the economy is described by a standard Cobb-Douglas production function with labor-augmenting technological progress, that is,

$$Y_t^{\text{Gross}} = K_t^{\alpha} (A_t L_t)^{1-\alpha}, \tag{2}$$

where α represents elasticity of substitution of capital, and A_t is a deterministic trend (cf. Appendix A). There is an externality to production in the form of industrial carbon emissions, $E_{\text{Ind},t}$, that reads as

$$E_{\text{Ind},t} = \sigma_t (1 - \mu_t) Y_t^{\text{Gross}}. \tag{3}$$

Through the emission flow, the economic side of our IAM affects the climate module (cf. Section 3.2 below). We follow Nordhaus (2017) and assume that the emissions produced are proportional to the final output, and scaled with an exogenous emission intensity σ_t. In our model, the emissions can be abated, that is, reduced, at a rate $\mu_t \in [0, 1]$. A zero abatement rate corresponds to the business-as-usual (BAU) case, whereas a value of $\mu = 1$, abatement corresponds to full mitigation.[11] As Nordhaus (2017), we assume that abatement is costly for the social planner and depends on the abatement rate with the following functional form:

$$\Theta_t(\mu_t) = \theta_{1,t} \mu_t^{\theta_2}. \tag{4}$$

In Eq. (4), $\theta_{1,t}$ is an exogenous process for the evolution of the abatement cost, and θ_2 is a parameter of the abatement cost function (see Appendix A for more details).

The unabated emissions enter the climate system and ultimately lead to an increase in the atmospheric temperature $T_{AT,t}$ (cf. Section 3.2). A rise in the atmospheric

[11] Note that in this augmented Ramsey model with climate externality, the abatement rate is a choice variable for the social planner in addition to the standard choice of investment.

temperature triggers damages that, in turn, will affect the final output. In our modeling setup, we employ two types of damage function commonly used in the IAM literature. The first one denoted by, $\Omega_t^N\left(T_{\mathrm{AT},t}\right)$, is the quadratic damage function by Nordhaus (2017):

$$\Omega_t^N\left(T_{\mathrm{AT},t}\right) = \frac{1}{1+\pi_1 T_{\mathrm{AT},t}+\pi_2 T_{\mathrm{AT},t}^2}. \tag{5}$$

The second damage function we employ in our computation is the one by Weitzman (2012), denoted by $\Omega_t\left(T_{\mathrm{AT},t}\right)$, but enhance it with stochastic tipping:[12]

$$\Omega_t\left(T_{\mathrm{AT},t}\right) = 1 - \frac{1}{1+\left(\frac{1}{\psi_1}T_{\mathrm{AT},t}\right)^2+\left(\frac{1}{2\cdot TP_t}T_{\mathrm{AT},t}\right)^{6.754}}. \tag{6}$$

We follow Kotlikoff et al. (2021) and assume that climate tipping is denoted by the variable TP_t that follows a random walk[13] with the Gaussian innovations with zero mean and variance equal to S_{TP}:[14]

$$TP_{t+1} = TP_t + \epsilon_{TP,t+1}, \quad \epsilon_{TP,t} \sim \mathcal{N}\left(0, S_{TP}\right). \tag{7}$$

The abatement costs and the damages jointly reduce the gross output of the economy. Thus the budget constraint reads as follows:

$$\left(1-\Theta_t\left(\mu_t\right)\right)\Omega_t\left(T_{\mathrm{AT},t}\right)Y_t^{\mathrm{Gross}} - C_t - I_t = 0. \tag{8}$$

[12] Climate tipping is the occurrence of climate events that lead to irreversible damages to the environment. For more details, see, e.g., Lenton et al. (2008), and references therein.

[13] The original work by Weitzman (2012) calibrates $2\cdot TP_t = 6.081$ to be constant over time. The climate tipping event occurs at about 3 C° excess temperature in the atmosphere. While the temperature change is below 3 C°, the climate tipping damage is negligibly small in the damage function. However, when it exceeds around 3 C°, the climate tipping damage begins to dominate the damage function. Our way of modeling the tipping in a stochastic way reflects the fact that very little is known about the exact level of temperatures at which tipping could occur (see Cai and Lontzek (2019), and references therein).

[14] In our computations below, we will truncate the normal distribution given in Eq. (7) to ensure numerical tractability (cf. Appendix A.2).

3.2 The climate model

In our modeling setup, we employ a climate emulator following the specification of Folini et al. (2023). This emulator is built on Nordhaus (2017) and comprises two fundamental building blocks: i) three stacked carbon reservoirs, i.e., boxes, that represent the global carbon cycle and ii) a two-layer energy balance model.

There are two sources of emissions that enter the simple carbon cycle: industrial emissions $E_{\text{Ind},t}$, as defined in Eq. (3), which are related to the economic activity of the representative agent, and exogenous emissions $E_{\text{Land},t}$. Their sum $E_t = E_{\text{Ind},t} + E_{\text{Land},t}$ constitutes the total emission flow entering the carbon cycle.

The three carbon reservoirs are represented by a three-dimensional vector $\mathbb{M}_t = (M_{\text{AT},t}, M_{\text{UO},t}, M_{\text{LO},t})$, where the entries represent the mass of carbon in the atmosphere (AT), upper ocean (UO) and lower ocean (LO) respectively. The concentration of carbon in those three boxes evolves according to a diffusion process described by the following expression:

$$\mathbb{M}_{t+1} = B\mathbb{M}_{t+1} + E_t, \tag{9}$$

where B is given by

$$B = \begin{pmatrix} 1 - b_{12} & b_{21} & 0 \\ b_{12} & 1 - b_{21} - b_{23} & b_{32} \\ 0 & b_{23} & 1 - b_{32} \end{pmatrix}. \tag{10}$$

The diffusion coefficients $b_{12}, b_{21}, b_{23}, b_{32}$ that we will use in our calculations are based on the calibration in Folini et al. (2023).

The baseline energy balance system–which we will have to slightly modify in Section 3.3–comprises two layers: the temperature of the atmosphere, $T_{\text{AT},t}$ (representing the atmosphere and upper ocean), and the temperature of the ocean, $T_{\text{OC},t}$, which are

described by the following equations:

$$T_{\mathrm{AT},t+1} = \left(1 - c_1 c_3 - c_1 \frac{F_{2\mathrm{xco2}}}{\Delta T_{\mathrm{AT},\times 2}}\right) T_{\mathrm{AT},t} + c_1 c_3 T_{\mathrm{OC},t} + c_1 \left(F_{2\mathrm{xco2}} \log_2 \left(\frac{M_{\mathrm{AT},t}}{M^*_{\mathrm{AT}}}\right) + F_{\mathrm{EX},t}\right) \tag{11}$$

$$T_{\mathrm{OC},t+1} = c_4 T_{\mathrm{AT},t} + (1 - c_4)\, T_{\mathrm{OC},t}. \tag{12}$$

$F_{2\mathrm{xco2}}$ denotes the forcing of equilibrium CO_2 doubling, $\Delta T_{\mathrm{AT},\times 2}$ is the ECS, M^*_{AT} starts for the equilibrium mass of carbon in the atmosphere, $F_{\mathrm{EX},t}$ represents exogenous radiative forcing, and c_1, c_3, c_4 are temperature-related parameters. All values, except the ECS, are calibrated according to Folini et al. (2023). A detailed discussion about the ECS follows in Section 3.3. More details on the calibration of our climate model are given in Appendix A.2.

3.3 Bayesian learning over the equilibrium climate sensitivity

The climate response in the form of the increase in atmospheric temperature to emissions (cf. Section 3.2) is subject to uncertainty in many ways. However, the ECS is presumably the most controversial number that determines how severe climate change will be in the long run (Knutti et al., 2017), as arguments between Roe and Baker (2007) and Zaliapin and Ghil (2010) in the climate science community illustrate. Therefore, to take state-of-the-art climate science seriously in our IAM, Eq. (11) has to be modified appropriately.

Empirical observations, as well as studies based on energy-balanced models and global climate models, suggest that the probability density function of the ECS is most likely to peak in the region $[2.0°\mathrm{C}, 4.5°\mathrm{C}]$, but exhibits a highly skewed and fat-tailed distribution (Roe and Baker, 2007). The latter authors, among others, pointed out that the ECS, $T_{\mathrm{AT},\times 2}$, relates to the following feedback process:

$$T_{\mathrm{AT},\times 2} = \frac{T^0_{\mathrm{AT},\times 2}}{1 - f}, \tag{13}$$

where f denotes the so-called climate feedback parameter, and $T^0_{\mathrm{AT},\times 2}$ is a reference cli-

mate sensitivity parameter, and which is known to the social planner. The uncertainty in the equilibrium climate sensitivity $T_{\mathrm{AT},\times 2}$ can be represented as the uncertainty in the climate feedback parameter f. Following Roe and Baker (2007), we assume that f follows a Gaussian distribution. By substituting Eq. (13) into Eq. (11), we obtain

$$T_{\mathrm{AT},t+1} = \left(c_1 \frac{F_{2\mathrm{xco2}}}{\Delta T^0_{\mathrm{AT},\times 2}} f + 1 - c_1 c_3 - c_1 \frac{F_{2\mathrm{xco2}}}{\Delta T^0_{\mathrm{AT},\times 2}} \right) T_{\mathrm{AT},t} + c_1 c_3 T_{\mathrm{OC},t} + c_1 \left(F_{2\mathrm{xco2}} \log_2 \left(\frac{M_{\mathrm{AT},t}}{M^*_{\mathrm{AT}}} \right) + F_{\mathrm{EX},t} \right) + \epsilon_{T,t+1}, \quad (14)$$

where the uncertainty about the ECS is now modeled indirectly via f. Following the literature, we introduce the Gaussian distributed shock $\epsilon_{T,t+1} \sim \mathcal{N}(0, S_{\epsilon_T})$, which the social planner cannot observe.

Following a seminar strand of literature on Bayesian learning in IAMs (see, e.g., Kelly and Kolstad (1999), Leach (2007), Webster et al. (2008), Kelly and Tan (2015), Hwang et al. (2017), Fitzpatrick and Kelly (2017)), we update the social planner's belief on the climate feedback parameter, not the ECS parameter, which is uncertain to the social planner. The social planner subjectively assumes his belief on the climate feedback parameter in period t, $\tilde{f}_{t+1}$, when solving the dynamic programming problem. As Roe and Baker (2007) suggest,[15] we assume that his prior belief on $\tilde{f}_{t+1}$ follows a Gaussian distribution with mean $\mu_{f,t}$ and variance $S_{f,t}$. We also assume that the distribution is truncated from below at $\underline{f} = 0.4$ and from above at $\overline{f} = 0.9$. This means $\tilde{f}_{t+1} \sim \mathcal{N}\left(\mu_{f,t}, S_{f,t}, \underline{f}, \overline{f}\right)$, and leads to an enhanced expression for the evolution of the atmospheric temperature, that is,

$$T_{\mathrm{AT},t+1} = \left(c_1 \frac{F_{2\mathrm{xco2}}}{\Delta T^0_{\mathrm{AT},\times 2}} \tilde{f}_{t+1} + 1 - c_1 c_3 - c_1 \frac{F_{2\mathrm{xco2}}}{\Delta T^0_{\mathrm{AT},\times 2}} \right) T_{\mathrm{AT},t} + c_1 c_3 T_{\mathrm{OC},t} + c_1 \left(F_{2\mathrm{xco2}} \log_2 \left(\frac{M_{\mathrm{AT},t}}{M^*_{\mathrm{AT}}} \right) + F_{\mathrm{EX},t} \right) + \tilde{\epsilon}_{T,t+1}. \quad (15)$$

[15] We take initial values for the prior mean and prior variance as in Roe and Baker (2007). With this, we need to take a value of a reference climate sensitivity $\Delta T^0_{\mathrm{AT},\times 2} = 1.2°\mathrm{C}$. This value, together with the starting value of the prior mean to a large extent, corresponds to our baseline calibration of the ratio between radiative forcing that is $F_{2\mathrm{xco2}} = 3.45\mathrm{W/m}^2$ and equilibrium climate sensitivity that is $\Delta T_{\mathrm{AT},\times 2} = 3.25°\mathrm{C}$.

In period t, we denote the prior probability function of the social planner's belief of the climate feedback parameter, which follows the Gaussian distribution with mean μ_t^f and variance $S_{f,t}$, as $p(f)$. Given the prior $p(f)$, the planner observes the atmospheric temperature change and the likelihood function of which is also given as a Gaussian $p(T_{\text{AT}} \mid f)$. By applying Bayes' rule, the posterior probability function of the climate feedback parameter given the observation T_{AT} is also Gaussian distributed, and reads as:

$$p(f \mid T_{\text{AT}}) \propto p(T_{\text{AT}} \mid f) \times p(f) \tag{16}$$

Following Kelly and Tan (2015), we rewrite the two stochastic components in Eq. (15) as

$$\left(1 - c_1 c_3 - c_1 \frac{F_{2\text{xco2}}}{\Delta T^0_{\text{AT},\times 2}}\right) T_{\text{AT},t} + c_1 c_3 T_{\text{OC},t} + c_1 \left(F_{2\text{xco2}} \log_2 \left(\frac{M_{\text{AT},t-1}}{M^*_{\text{AT}}}\right) + F_{\text{EX},t}\right) + \varphi_{1\text{C}} \tilde{f}_{t+1} T_{\text{AT},t} + \tilde{\epsilon}_{T,t+1} - T_{AT,t+1} = 0, \tag{17}$$

where $\varphi_{1\text{C}} = c_1 \frac{F_{2\text{xco2}}}{\Delta T^0_{\text{AT},\times 2}}$, and where $\tilde{f}_{t+1} \sim \mathcal{N}\left(\mu_{f,t}, S_{f,t}, \underline{f}, \overline{f}\right)$, $\tilde{\epsilon}_{T,t+1} \sim \mathcal{N}(0, S_{\epsilon^T})$. Finally, by applying DeGroot (1970, p. 167, Theorem 1), we can analytically compute the posterior mean and the variance, that is,

$$\mu_{f,t+1} = \frac{S_{\epsilon_T} \mu_{f,t} + \varphi_{1\text{C}} T_{\text{AT},t} \left(\varphi_{1\text{C}} T_{\text{AT},t} \tilde{f}_{t+1} + \tilde{\epsilon}_{T,t+1}\right) S_{f,t}}{S_{\epsilon_T} + \left(\varphi_{1\text{C}} T_{\text{AT},t}\right)^2 S_{f,t}} \tag{18}$$

$$S_{f,t+1} = \frac{S_{\epsilon_T} S_{f,t}}{S_{\epsilon_T} + \left(\varphi_{1\text{C}} T_{\text{AT},t}\right)^2 S_{f,t}}. \tag{19}$$

3.4 The recursive formulation

After putting all building blocks in place in Sections 3.1 to 3.3, we now present the recursive formulation of our IAM with Bayesian learning about the ECS. The social

planner choices consumption C_t, investment K_{t+1} and mitigation $\mu_t \in [0,1]$ to solve

$$V(\boldsymbol{X}_t)^{1-1/\psi} = \max_{C_t, K_{t+1}, \mu_t} \left\{ \left(\frac{C_t}{L_t} \right)^{1-1/\psi} L_t + e^{-\rho} \mathbb{E}_t \left[V(\boldsymbol{X}_{t+1})^{1-\gamma} \right]^{\frac{1-1/\psi}{1-\gamma}} \right\} \tag{20}$$

$$\text{s.t.} \quad (1 - \Theta(\mu_t)) \, \Omega_t(T_{\mathrm{AT},t}) \, K_t^{\alpha} (A_t L_t)^{1-\alpha} - C_t - I_t = 0 \tag{21}$$

$$(1-\delta) K_t + I_t - K_{t+1} = 0 \tag{22}$$

$$1 - \mu_t \geq 0 \tag{23}$$

$$(1 - b_{12}) M_{\mathrm{AT},t} + b_{21} M_{\mathrm{UO},t} + (1-\mu_t) \sigma_t K_t^{\alpha} (A_t L_t)^{1-\alpha} + E_{\mathrm{Land},t} - M_{\mathrm{AT},t+1} = 0 \tag{24}$$

$$b_{12} M_{\mathrm{AT},t} + (1 - b_{21} - b_{23}) M_{\mathrm{UO},t} + b_{32} M_{\mathrm{LO},t} - M_{\mathrm{UO},t+1} = 0 \tag{25}$$

$$b_{23} M_{\mathrm{UO},t} + (1 - b_{32}) M_{\mathrm{LO},t} - M_{\mathrm{LO},t+1} = 0 \tag{26}$$

$$\begin{aligned} &(1 - c_1 c_3 - \varphi_{1C}) T_{\mathrm{AT},t} + c_1 c_3 T_{\mathrm{OC},t} + c_1 \left(F_{2\mathrm{xco2}} \log_2 \left(\frac{M_{\mathrm{AT},t}}{M^*_{\mathrm{AT}}} \right) + F_{\mathrm{EX},t} \right) \\ &\quad + \varphi_{1C} \tilde{f}_{t+1} T_{\mathrm{AT},t} + \epsilon_{T,t+1} - T_{\mathrm{AT},t+1} = 0 \end{aligned} \tag{27}$$

$$c_4 T_{\mathrm{AT},t} + (1 - c_4) T_{\mathrm{OC},t} - T_{\mathrm{OC},t+1} = 0 \tag{28}$$

$$\frac{S_{\epsilon_T} \mu_{f,t} + \varphi_{1C} T_{\mathrm{AT},t} \left(\varphi_{1C} T_{\mathrm{AT},t} \tilde{f}_{t+1} + \epsilon_{T,t+1} \right) S_{f,t}}{S_{\epsilon_T} + (\varphi_{1C} T_{\mathrm{AT},t})^2 S_{f,t}} - \mu_{f,t+1} = 0 \tag{29}$$

$$\frac{S_{\epsilon^T} S_{f,t}}{S_{\epsilon^T} + (\varphi_{1C} T_{\mathrm{AT},t})^2 S_{f,t}} - S_{f,t+1} = 0 \tag{30}$$

$$\tilde{f}_{t+1} \sim \mathcal{N}\left(\mu_{f,t}, S_{f,t}, \underline{f}, \overline{f} \right), \epsilon_{T,t+1} \sim \mathcal{N}(0, S_{\epsilon^T}) \tag{31}$$

$$\Omega(T_{\mathrm{AT},t}) = 1 - \frac{1}{1 + \left(\frac{1}{20.46} T_{\mathrm{AT},t} \right)^2 + \left(\frac{1}{2 \cdot TP_t} T_{\mathrm{AT},t} \right)^{6.754}} \tag{32}$$

where the Bellman equation, given by Eq. (20) is subject to the budget constraint Eq. (21), the occasionally binding upper bound on mitigation variable μ_t, the three laws of motion of the carbon concentration in the atmosphere Eq. (24), in the upper ocean Eq. (25) and in the lower ocean Eq. (26), the two laws of motion of the atmospheric temperature Eq. (27) and the ocean temperature Eq. (28), the Bayesian updates of the ECS, and the stochastic motion of the damage coefficients.

In Eq. (20), the the state of the model is given by $\boldsymbol{X}_t = (K_t, \boldsymbol{\Gamma}_t, \boldsymbol{S}_t, TP_t, t; \boldsymbol{\vartheta})$, where $\boldsymbol{\Gamma}_t = (M_{\mathrm{AT},t}, M_{\mathrm{UO},t}, M_{\mathrm{LO},t}, T_{\mathrm{AT},t}, T_{\mathrm{OC},t})$ denote the climate variables, $\boldsymbol{S}_t = \left(\mu_{f,t}, S_{f,t} \right)$ the mean and variance of the agent's beliefs, TP_t the climate tipping state, whereas t

abbreviates the state variable that handles time. Finally, $\boldsymbol{\vartheta}$ is a collection of N uncertain parameters $\boldsymbol{\vartheta} = (\vartheta_1, \cdots \vartheta_N)$, which we consider pseudo-state variables (Scheidegger and Bilionis, 2019), and over which the planner, in contrast to the other stochastic variables, does not compute expectations. Thus, the total dimensionality d of the IAM, therefore, is given by:

$$d = |K_t| + |\boldsymbol{\Gamma}_t| + |\boldsymbol{S}_t| + |TP_t| + |t| + |\boldsymbol{\vartheta}| = 1 + 5 + 2 + 1 + 1 + N = 10 + N. \tag{33}$$

4 Deep uncertainty quantification

In what follows, we introduce our Deep UQ methodology in three steps. First, we outline in Section 4.1 how "Deep Equilibrium Nets" (DEQN) can be adapted to compute global solutions to (non-stationary) stochastic IAM model as a function of its economic and climate states, as well as parameters (Section 4.1.1), and how the resulting optimal policies can subsequently be used to construct cheap-to-evaluate surrogate models for derived quantities of interest, such as the SCC, by using the Gaussian process-based surrogated model (Section 4.1.2). Section 4.2 introduces the global sensitivity measures we intend to study in the context of our IAM. Section 4.3 finally presents the Deep UQ algorithm formally. Additional details of the implementation are found in Appendix B.

4.1 Surrogate models for IAMs

4.1.1 Deep equilibrium nets

In this section, we briefly summarize the general idea of DEQN, thereby adopting the notation of Azinovic et al. (2022), Folini et al. (2023). The DEQN algorithm is a simulation-based solution method using deep neural networks to compute an approximation of the *optimal policy function* $\mathbf{p} : X \rightarrow Y \subset \mathbb{R}^M$ to a dynamic model under the assumption that the underlying economy can be characterized via discrete-time first-order equilibrium conditions, that is,

$$\boldsymbol{G}(\mathbf{x}, \mathbf{p}) = \mathbf{0}, \ \forall \mathbf{x} \in X \subset \mathbb{R}^d. \tag{34}$$

Intuitively, DEQNs work as follows: An unknown policy function is approximated with a neural network, that is, $\mathbf{p}(\boldsymbol{x}) \approx \mathcal{N}(\boldsymbol{x})$, and where the $\boldsymbol{\nu}$'s are ex-ante unknown coefficients of the neural network that have to be determined based on some suitable loss function measuring the quality of a given approximation at a given state of the economy.

Although there are several different types of deep neural networks, we use in this paper the so-called densely-connected feedforward neural networks (FNN).[16] Following the literature, we define an L-layer FNN as a function $\mathcal{NN}^L(\boldsymbol{x}) : \mathbb{R}^{d_{\text{input}}} \to \mathbb{R}^{d_{\text{output}}}$ and say that there are $L-1$ hidden layers such that the ℓ-th layer has N_ℓ neurons. In our concrete case, $K = N_0 = d_{\text{in}}$ and $M = N_L = d_{\text{output}}$.[17] Furthermore, for each $1 \leq \ell \leq L$, we define a so-called weight matrix $\boldsymbol{W}^\ell \in \mathbb{R}^{N_\ell \times N_{\ell-1}}$ and bias vector $\boldsymbol{b}^\ell \in \mathbb{R}^{N_\ell}$. Then, letting $A^\ell(\boldsymbol{x}) = \boldsymbol{W}^\ell \boldsymbol{x} + \boldsymbol{b}^\ell$ be the affine transformation in the ℓ-th layer, for some non-linear activation function $\sigma(\cdot)$ such as relu, swish, or selu, an FNN is given by

$$\mathbf{p}(\mathbf{x}) \approx \mathcal{N}(\mathbf{x}) = \mathcal{N}^L(\mathbf{x}) = A^L \circ \sigma_{L-1} \circ A^{L-1} \circ \ldots \circ \sigma_1 \circ A^1(\mathbf{x}). \tag{35}$$

In Section 4.1.1, we illustrate a simple FNN with two hidden layers. The selection of hyper-parameters $\left\{L, \{N_l\}_{l=1}^L, \{\sigma_l(\cdot)\}_{l=1}^L\right\}$ is known as the architecture selection. Approaches to determine these hyper-parameters include using prior experience, manual, random, or grid search, as well as more complex methods such as Bayesian optimization (see, e.g., Bergstra et al. (2011)).

The DEQN algorithm to determine $\mathbf{p}(\mathbf{x})$ is started by randomly initializing the ν's (Glorot and Bengio, 2010), that is, an arbitrary guess for the ex-ante unknown approximate policy function. Next, we simulate a sequence of $N_{\text{path length}}$ states. Starting from some given state $\mathbf{x}_t$, the next state $\mathbf{x}_{t+1}$ is the result of the policies encoded by the neural network, $\mathcal{N}(\mathbf{x})$, and remaining, model-implied dynamics.

If we knew the (approximate) policy function satisfying the equilibrium conditions,

[16] Neural networks are universal function approximations (Hornik et al., 1989) and can resolve highly non-linear features, and can handle a large amount of high-dimensional input data. See, e.g., Goodfellow et al. (2016) for an excellent introduction to deep learning.

[17] Recall that in our model, we $d_{\text{in}} = d = 10 + N$ input dimensions (cf. Eq. (33)). Furthermore, $d_{\text{output}} = 3$, as we have our model has three choice variables, these are, consumption, investment, and mitigation (cf. Section 3.4).

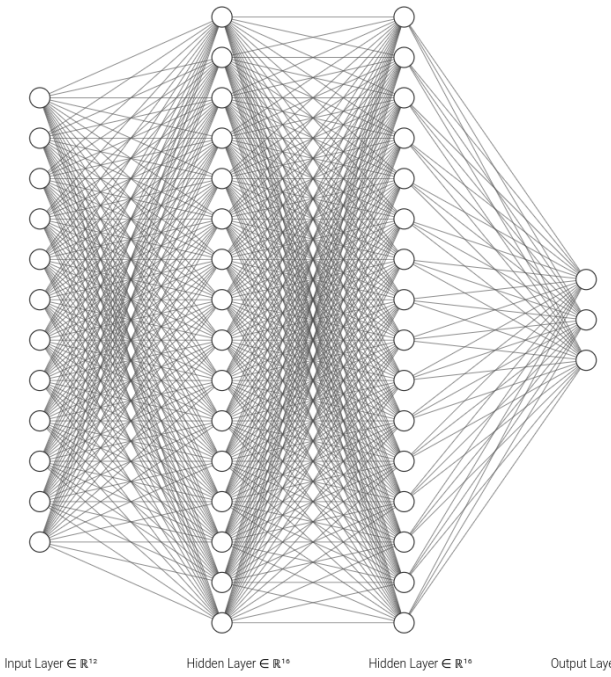

Figure 1: The figure above depicts an FNN, where the input $\mathbf{x}$ is a 12−dimensional vector, two hidden layers with 16 neurons each, and $\mathbf{p}(\mathbf{x})$ is a 3−dimensional output, thereby representing a stylized architecture for an IAM with 10 economic state variables, two parameters that are considered as pseudo-states, and three control variables (cf. Eq. (33)).

Eq. (34) would hold along a simulated path. However, since the neural network is initialized with random coefficients, $\boldsymbol{G}(\mathbf{x}_t, \mathcal{N}(\mathbf{x}_t)) \neq 0$ along the simulated path of length $N_{\text{path length}}$. This fact is now leveraged to improve the quality of the guessed policy function. Specifically, DEQNs use a loss function as the error in the equilibrium conditions, that is,

$$\ell_{\boldsymbol{\nu}} := \frac{1}{N_{\text{path length}}} \sum_{\mathbf{x}_t \text{on sim. path}} \sum_{m=1}^{N_{\text{eq}}} \left(\boldsymbol{G}_m(\mathbf{x}_t, \mathcal{N}(\mathbf{x}_t))\right)^2, \tag{36}$$

where $\boldsymbol{G}_m(\mathbf{x}_t, \mathcal{N}(\mathbf{x}_t))$ represent all the N_{eq} first-order equilibrium conditions of a given model, that is, $\boldsymbol{G}(\mathbf{x}_t, \mathcal{N}(\mathbf{x}_t)) = \sum_{m=1}^{N_{\text{eq}}} (\boldsymbol{G}_m(\mathbf{x}_t, \mathcal{N}(\mathbf{x}_t))$. Eq. (36) can now be used to update

the weights of the network with any variant of gradient descent,[18] namely,

$$\nu_k' = \nu_k - \alpha^{\text{learn}} \frac{\partial \ell(\boldsymbol{\nu})}{\partial \nu_k}, \tag{37}$$

where ν_k' represents the updated $k-$th weight of the neural network, and where $\alpha^{\text{learn}} \in \mathbb{R}$ denotes the so-called learning rate. The updated neural network-based representation of the policy is subsequently used to simulate a sequence of length $N_{\text{path length}}$ steps, along which the loss function is recorded, and the latter is again used to update the network parameters. This iterative procedure is pursued until $\ell_{\boldsymbol{\nu}} < \epsilon \in \mathbb{R}$, that is, an approximate equilibrium policy, has been found.

In summary, the DEQN algorithm consists of four building blocks: i) deep neural networks for approximating the equilibrium policies; ii) a suitable loss function measuring the quality of a given approximation at a given state of the economy; iii) an updating mechanism to improve the quality of the approximation; and iv) a sampling method for choosing states for updating and evaluating of the approximation quality. In Appendix B.1, the step-by-step procedure for mapping stochastic and non-stationary climate economic models in general, and our model in particular, onto the neural network-based DEQN solution framework is provided.

4.1.2 Gaussian process surrogate models for global sensitivity analysis

We now briefly introduce the Gaussian process regression (GPR), a probabilistic approach for modeling a regression problem[19] that we will use below to construct surrogates for approximating and interpolating QoIs, such as the SCC, as a function of the model input parameters, to enable the swift computation of global sensitivity measures such as the Sobol' indices, the univariate effects and the Shapley values (cf. Section 4.2 below).

GPR assumes that the underlying function is a sample from a GP. The latter is defined by a mean function, $m(x)$, and a covariance function, $k(x, x')$. For a regression problem, we are given a set of n input-output pairs, $\mathcal{D} = \{x_i, y_i\}_{i=1}^n = [X, y]$, where

[18] In our practical applications, we use "Adam"(Kingma and Ba, 2014).
[19] See, e.g., Rasmussen and Williams (2005) for a textbook treatment.

$x_i \in \mathbb{R}^d$, $y_i \in \mathbb{R}$, $X \in \mathbb{R}^{n \times d}$ and $y \in \mathbb{R}^{n \times 1}$, and to which the literature also refers to as " training dataset" or "experimental design".[20] The goal is to "learn", that is, approximate a function $f(x)$ that maps inputs to outputs. In GPR, one often assumes that the output y is generated by a noisy evaluation of the function $f(x)$, i.e., $y = f(x) + \epsilon$, where $\epsilon \sim \mathcal{N}\left(0, \sigma_\epsilon^2\right)$, as it renders the computations numerically more stable (see, e.g., Rasmussen and Williams (2005), Murphy (2012)).

The prior distribution over functions is given by a GP, that is, $f(x) \sim \mathcal{GP}(m(x), k(x, x'))$. In practical applications, the mean function, $m(x)$, is often set to a constant value, e.g., zero. The covariance function, $k(x, x')$, defines the correlation between two arbitrary inputs x and x'. The exact choice of the kernel within an application depends on how the modeler encodes prior knowledge about the function(s) to be approximated, such as differentiability and periodicity. In our work below, we use the Matérn 5/2 kernel, which is given by:

$$k(x, x') = \sigma_f^2 \left(1 + \frac{\sqrt{5}r}{\rho} + \frac{5r^2}{3\rho^2}\right) \exp\left(-\frac{\sqrt{5}r}{\rho}\right), \tag{38}$$

where σ_f^2 denotes the variance parameter, and ρ represents the length scale parameter. The distance r between x and x' can be calculated using a suitable metric, such as the Euclidean distance.[21]

Given the input-output pairs in $\mathcal{D}$, we can compute the posterior distribution over functions using Bayes' rule, that is,

$$p(f_* \mid x_*, \mathcal{D}) = \mathcal{N}\left(\mu_*, \sigma_*^2\right), \tag{39}$$

where x_* is an arbitrary point from the computational domain (also referred to as "test input"), f_* is the corresponding output, and μ_* and σ_*^2 are the mean and variance of

[20] Below, the input vector x_i will be given by the vector of parameters of dimensionality N (cf. Eq. (33)), whereas corresponding observations y_i will represent the QoIs.

[21] Note that the hyperparameters of the covariance function are typically estimated by maximizing the likelihood (Rasmussen and Williams, 2005). For more details on kernels, see, e.g., Murphy (2022, Ch. 18.2).

the predictive distribution. They can be computed as:

$$\mu_*(x_*) = k(x_*, X)\left[K(X, X) + \sigma_\epsilon^2 I\right]^{-1} y, \tag{40}$$

$$\sigma_*^2(x_*) = k(x_*, x_*) - k(x_*, X)[K(X, X) + \sigma_\epsilon^2 I]^{-1} k(X, x_*), \tag{41}$$

where $K(X, X')$ is the matrix of pairwise covariances between inputs in X and X'. Furthermore, I is an identity matrix and σ_ϵ is the assumed noise level of observations, that is, the variance of ϵ. Thus, the interpolation value of a function at a location x_* is given by $f(x_*) = \mu_*$. For more details on GPs, see, e.g., Renner and Scheidegger (2018), and references therein.

Below, we require cheap-to-evaluate GP surrogates for one particular QoI as a function of the model input parameters that is relevant to the climate policy and for which we intend to perform global sensitive analysis at any given point in time. SCC is defined as the marginal cost of atmospheric carbon in terms of the numeraire good. Following the literature (see, e.g., Traeger (2014)), we define SCC as the marginal rate of substitution between atmospheric carbon concentration of a 1000 Gt of carbon where c2co2 represents carbon to CO_2 transformation coefficient[22] and the normalized capital stock, that is,

$$SCC_t = \frac{-\left(\partial V_t / \partial M_{\mathrm{AT},t}\right) / \mathrm{c2co2}}{\partial V_t / \partial K_t} = \frac{-\left(\partial v_t / \partial M_{\mathrm{AT},t}\right) / \mathrm{c2co2}}{\partial v_t / \partial k_t} A_t L_t. \tag{42}$$

To enable a comparison to related studies, we focus below on the SCC in the year 2100, a date commonly used in the literature (see, e.g., Cai and Lontzek (2019)), that is,

$$y_{\mathrm{SCC}} = \mathbb{E}\left[\mathrm{SCC}_{2100}\right]. \tag{43}$$

To construct the GP surrogates of the QoI mentioned above as a function of the model input parameters ϑ, we proceed as follows:[23] Suppose that we observe n_s

[22] The stock of carbon in the carbon cycle is measured in 1000 Gt of carbon; however, the backstop cost as in Nordhaus (2017) is measured in 1000 Gt of CO_2 emissions; thus, to obtain a correct value for SCC, we need to transform a value measured in carbon into CO_2 by the transformation coefficient c2co2 = 3.666.

[23] In Section 4.1.2, we generally introduce the GPR that is trained on a set of n input-output pairs, which is $\mathcal{D} = \{x_i, y_i\}_{i=1}^n = [X, y]$. Hereafter we focus more on our specific case where the mode input

model input-output pairs, we obtain a training set, or experimental design, $\mathcal{D}_s = \{\boldsymbol{\vartheta}_i, y_i\}_{i=1}^n = [\Theta_s, y_s]$ consisting of n sample vectors $\boldsymbol{\vartheta}_i \in \mathbb{R}^N$ from a joint (uniform) distribution of the uncertain model parameters, whereas $y_i \in \mathbb{R}$ corresponds to the QoI at a given combination of parameters and can be generated by interpolating on the DEQN surrogate of the pre-computed IAM solution (cf. Eq. (35)). Next, we fit a GP model to the training data set $\mathcal{D}_s$ and write it as $\mathcal{M}_{\text{GP}|\Theta_s,y_s}$. Note that the fitted GP surrogate model (or GP metamodel) is *cheap-to-evaluate* and predicts the model responses with a negligible computation time. We use the predictive mean, $\mu_*(\boldsymbol{\vartheta})$, of the respective GP model that we denote by $\mathcal{M}_{\text{GP}|\Theta_s,y_s}$, as the interpolation value for the respective QoI, that is, y_{SCC}. [24] Evaluating $\mu_*(\cdot)$ numerically is extremely fast, as the algorithmic complexity is linearly in the size n of the training data set (cf. Eq. (40)). Thus, global sensitivity analysis of very rich specified models (cf. Section 4.2) now becomes numerically tractable. More details regarding the accuracy of GP surrogate models are provided in Appendix C.

4.2 Global sensitivity analysis in a nutshell

In this section, we present a formal introduction to surrogate-based global sensitivity analysis (GSA).

4.2.1 Some definitions

We begin our discussion of GSA by introducing essential notation, following the notation set forth by Saltelli et al. (2007), Sudret (2008) and Harenberg et al. (2019). Let us define a (true) mathematical model $\mathcal{M}(\cdot)$ that maps

$$\boldsymbol{\vartheta} \in \mathcal{D}_{\boldsymbol{\vartheta}} \subset \mathbb{R}^N \rightarrow y = \mathcal{M}(\boldsymbol{\vartheta}) \in \mathbb{R}, \tag{44}$$

parameters are denoted by ϑ_i, not x_i and define the n input-output pairs $\mathcal{D}_s = \{\vartheta_i, y_i\}_{i=1}^n = [\Theta_s, y_s]$.

[24] Note that the GP surrogate is redundant when a QoI is not a derived quantity from the optimal policies such as μ_t. In contrast, where a QoI relies on simulations such as the SCC, constructing a GP-based surrogate can reduce the computational burden substantially since next to evaluating the exact formula of the SCC at n points to train a GP, everywhere else in the parameter space, the respective quantity can be retrieved by evaluating the surrogate model.

where y is called a quantity of interest (QoI)[25] that is, a random endogenous outcome of the computational model $\mathcal{M}(\cdot)$, where $\boldsymbol{\vartheta} = (\vartheta_1, \cdots, \vartheta_N)$ is the random vector of N input parameters, where each of which is characterized by a probability density function (PDF) $f_{\vartheta_i}, i = 1, \cdots, N$, and where the joint density $f_{\boldsymbol{\vartheta}}$ is defined over a probabilistic space (see, e.g., Jaynes (1957, 1982)). The corresponding ex-ante unknown distribution of the endogenous output y is inferred by evaluating the model on a large sample of parameter values drawn from the specified distribution $f_{\boldsymbol{\vartheta}}$, a technique that is termed *uncertainty propagation* (see, e.g., Sudret (2008) and references therein). Based on this distribution, we next look at three particular types of metrics that are typically studied in the UQ literature, namely, the Sobol' indices (Section 4.2.2), the univariate effects (Section 4.2.3), and the Shapley values (Section 4.2.4).

4.2.2 Sobol' indices

Variance-based GSA methods discriminate among all the model's parameters according to their contribution to the variance of its output. In our concrete case, we intend to study which (combinations of) parameters drive the QoI's volatility by applying Sobol's decomposition (Sobol, 2001). Following a common practice in the UQ literature, for instance, see Saltelli et al. (2007), we start from the Sobol's variance decomposition to investigate possible interactions among model inputs on the model output y, that is[26]

$$\text{Var}[y] = \sum_{i=1}^{N} V_i + \sum_{1 \leq i \leq j \leq N} V_{i,j} + \cdots + V_{1,2,\cdots,N}, \tag{45}$$

where $V_{\boldsymbol{u}}$ denotes the partial variances for any subset of parameter indices $\boldsymbol{u} \subset \{1, 2, \cdots, N\}$, and in particular in our case,

$$V_i = \text{Var}\left[\mathbb{E}\left[\mathcal{M}(\boldsymbol{\vartheta}) \mid \vartheta_i\right]\right], \tag{46}$$

[25] Recall that in our case, we consider the SCC as a function of the model parameters at a given point in time (cf. Eq. (42)).

[26] Sobol's decomposition is closely related to a function approximation technique called "high-dimension model representation" (see, e.g., Ma and Zabaras (2010), Eftekhari et al. (2017), Eftekhari and Scheidegger (2022), and references therein).

and

$$V_{i,j} = \mathrm{Var}\left[\mathbb{E}\left[\mathcal{M}\left(\boldsymbol{\vartheta}\right) \mid \vartheta_i, \vartheta_j\right]\right] - \mathrm{Var}\left[\mathbb{E}\left[\mathcal{M}\left(\boldsymbol{\vartheta} \mid \vartheta_i\right)\right]\right] - \mathrm{Var}\left[\mathbb{E}\left[\mathcal{M}\left(\boldsymbol{\vartheta} \mid \vartheta_j\right)\right]\right], \quad (47)$$

and so forth.

A natural extension to the relative shares of partial variances in the total variance leads to the well-known sensitivity measures, i.e., Sobol' indices (Sobol, 2001). For any subset of parameters' indices $\boldsymbol{u}$, the Sobol' index is defined as

$$S_{\boldsymbol{u}} = \frac{\mathrm{Var}_{\vartheta_{\boldsymbol{u}}}\left[\mathbb{E}_{\boldsymbol{\vartheta}\setminus\vartheta_{\boldsymbol{u}}}\left[\mathcal{M}\left(\boldsymbol{\vartheta}\right) \mid \vartheta_{\boldsymbol{u}}\right]\right]}{\mathrm{Var}_{\boldsymbol{\vartheta}}\left[Y\right]}. \quad (48)$$

The Sobol' indices given by Eq. (48) are indicators used in the variance-based sensitivity analysis (Sobol, 2001). In practical terms, Sobol' indices quantify which uncertain parameters and non-linear interactions among uncertain parameters primarily contribute to the variances of model outcomes. In other words, one can *screen* uncertain parameters to decrease overall model variance by investigating the Sobol' indices. In our work below, we particularly look at the first-order Sobol' index when we set $\boldsymbol{u} = \{i\}$ in Eq. (48), that is,

$$S_i = \frac{\mathrm{Var}_{\vartheta_i}\left[\mathbb{E}_{\boldsymbol{\vartheta}\setminus\vartheta_i}\left[\mathcal{M}\left(\boldsymbol{\vartheta}\right) \mid \vartheta_i\right]\right]}{\mathrm{Var}_{\boldsymbol{\vartheta}}\left[Y\right]}. \quad (49)$$

In our numerical examples below, we follow, among others, Oakley and O'Hagan (2004) and Marrel et al. (2009) and use the predictive mean of the fitted Gaussian process surrogate model $\mathcal{M}_{\mathrm{GP}|\Theta_s,Y_s}$ instead of the "true" $\mathcal{M}(\cdot)$ to enable a swift computation of GSA metrics (see, cf. Section 4.1.2).[27] To compute the first-order Sobol' indices defined in Eq. (49), we start by generating arbitrary big test data inputs $\Theta = \{\boldsymbol{\vartheta}_i\}_{i=1}^{N_\omega}$ on which we simulate the GP model $\mathcal{M}_{\mathrm{GP}|\Theta_s,y_s}$ for N_ω times to obtain the model predictions. The sample space Ω represents the possible model outcomes $\boldsymbol{\omega}$ from the posterior. We replace the model output $\mathcal{M}_i\left(\vartheta_i\right)$ by the mean of the posterior distribution and

[27] Next to GPs, polynomial chaos expansions is also commonly used in the literature to construct surrogate models for the swift computation of Sobol' indices (see, e.g., Sudret (2008), Harenberg et al. (2019)).

estimate the first-order Sobol' indices for parameter i (Marrel et al., 2009), that is,

$$S_i = \frac{\mathrm{Var}_{\vartheta_i}\mathbb{E}_{\Theta\setminus\vartheta_i}\left[\mathbb{E}_{\Omega}\left[\mathcal{M}_{\mathrm{GP}|\Theta_s,y_s}(\Theta)\right] \mid \vartheta_i\right]}{\mathrm{Var}_{\Theta}\mathcal{M}_{\mathrm{GP}|\Theta_s,y_s}(\Theta)}. \tag{50}$$

4.2.3 Univariate effects

From the aforementioned variance decomposition, we do not obtain any information as to which direction a QoI moves when the uncertain parameters deviate from their benchmark values. To this end, GSA is also concerned with computing univariate effects (Younes et al., 2013). Formally, a univariate effect represents the model's conditional expectation of QoI when we fix a single model parameter ϑ_i at an arbitrary point ϑ_i', where the expectations are taken over all other parameters, that is,

$$\mathcal{U}_i\left(\vartheta_i'\right) = \mathbb{E}_{\vartheta\setminus\vartheta_i}\left[\mathcal{M}(\vartheta) \mid \vartheta_i = \vartheta_i'\right] \tag{51}$$

As outlined in Section 4.2.2, we replace the true "true" $\mathcal{M}(\cdot)$ again by the GP surrogate model $\mathcal{M}_{\mathrm{GP}|\Theta_s,y_s}$, and evaluate the model outputs by using the posterior mean of the GP.

4.2.4 Shapley value

An essential task in UQ is to attribute the uncertainty of the overall outcome of the model to various input parameters. In the field of GSA, the Sobol' indices have been widely adopted for variance decomposition (Saltelli et al., 2007, Harenberg et al., 2019). On the other hand, the economic literature, especially in cooperative game theory, has studied a similar problem and developed a solution concept known as the Shapley value (Shapley, 1953, Winter, 2002). The key idea behind the Shapley value is to determine a fair way to attribute the value created by a team effort to each team member. Based on this insight, Owen (2014) introduced a global sensitivity measure that is based on the Shapley value, and shows that the Shapley value is a compelling choice for identifying how much model variance can be attributed to the uncertainty in input parameters.

Following Owen (2014), Song et al. (2016) and our previously introduced notation

we define a Shapley value for the i-th uncertain parameter as:

$$Sh_i = \sum_{\boldsymbol{u} \subseteq \mathcal{K} \setminus i} \frac{(N - |\boldsymbol{u}| - 1)!|\boldsymbol{u}|!}{N!} \left(\text{Var}\left[\mathcal{M}\left(\vartheta_{\boldsymbol{u} \cup \{i\}} \right) \right] - \text{Var}\left[\mathcal{M}\left(\vartheta_{\boldsymbol{u}} \right) \right] \right), \tag{52}$$

where $\mathcal{K} = \{1, 2, \cdots, N\}$, and $N = |\mathcal{K}|$ is the size of the whole set and $|\boldsymbol{u}|$ is the size of subset $\boldsymbol{u}$. We also define $\text{Var}\left[\mathcal{M}\left(\vartheta_{\emptyset} \right) \right] = 0$. Eq. (52) measures the incremental cost when including parameter i in set $\boldsymbol{u}$ averaged over all sets $\boldsymbol{u} \subseteq \mathcal{K} \setminus i$. Owen (2014) proposes to choose

$$\text{Var}\left[\mathcal{M}\left(\vartheta_{\boldsymbol{u}} \right) \right] = \text{Var}_{\vartheta_{\boldsymbol{u}}} \left[\mathbb{E}_{\mathcal{K} \setminus \boldsymbol{u}} \left[\mathcal{M}\left(\vartheta \right) | \vartheta_{\boldsymbol{u}} \right] \right], \tag{53}$$

with which one can measure a similar effect as the one of the first-order Sobol' indices. Another functional form of the cost function used in the literature is given by the following expression:

$$\text{Var}\left[\mathcal{M}\left(\vartheta_{\boldsymbol{u}} \right) \right] = \mathbb{E}_{\mathcal{K} \setminus \boldsymbol{u}} \left[\text{Var}_{\boldsymbol{u}} \left[\mathcal{M}\left(\vartheta \right) | \vartheta_{\mathcal{K} \setminus \boldsymbol{u}} \right] \right]. \tag{54}$$

Song et al. (2016) prove that the Shapley values using either the cost function in Eq. (53) or Eq. (54) are equivalent. Furthermore, when numerically estimating the Shapley value, Sun et al. (2011) pointed out that the Monte Carlo estimation of the inner expectation operator in Eq. (53) requires a sufficiently large number of model evaluations and could be highly biased. On the other hand, the estimation in Eq. (54) is unbiased for all sample sizes. Consequently, we use Eq. (54) in all our computations.

When the number of uncertain parameters N, as in our case, is reasonably "small", one typically uses the "exact" method by Song et al. (2016). The latter involves traversing $N!$ permutated sets. To enhance the efficiency of the Monte Carlo sampling required for precise evaluation of the expectation and variance operators, we again employ the GP-based surrogate model, thereby replacing the original model; that is, we utilize the predictive mean of the posterior for this purpose.[28]

[28] See Iooss and Prieur (2019) for more technical details.

4.3 The deep uncertainty quantification algorithm

After having discussed the ingredients to our "Deep UQ" methodology in Section 4.1 and Section 4.2, we now present code listing 1 the complete algorithm. It consists of two fundamental building blocks. First, the DEQN is used to solve the IAM as a function of all endogenous, exogenous, and pseudo-state variables in a single solution step. The resulting neural network-based surrogate model then serves as an input to construct Gaussian Process (GP) surrogates for QoI metrics, such as the SCC. Subsequently, UQ can be performed on these GP surrogates to assess and analyze the uncertainty in the model predictions.

Algorithm 1 Deep UQ algorithm

Part 1: Deep equilibrium nets

Approximate policy functions $\boldsymbol{p}(\boldsymbol{x}_t)$ using DEQN parametrized by the coefficients $\boldsymbol{\nu}$, where $\boldsymbol{x}_t \equiv [K_t, \boldsymbol{\Gamma}_t, \boldsymbol{X}_t, t; \boldsymbol{\vartheta}]$.

Input:

Neural network architecture and hyper-parameters, simulation length T (length of an episode), α^{learn} (learning rate), $\boldsymbol{x}_0$ (initial states). Upper and lower bound of the pseudo states $\boldsymbol{\vartheta} \in \left[\underline{\boldsymbol{\vartheta}}, \overline{\boldsymbol{\vartheta}}\right]$.

Output:

The neural network's trained parameters $\boldsymbol{\nu}^*$, such that the policy function $\boldsymbol{p}(\boldsymbol{x}_t) \approx \mathcal{N}(\boldsymbol{x}_t)$ minimizes the loss function, i.e., the system of the first-order equilibrium conditions.

while $\ell_{\boldsymbol{\nu}} > \epsilon$ **do**

$\boldsymbol{x}_0^i \leftarrow \boldsymbol{x}_0$ ▷ Initialize the states at time 0

$\mathcal{D}_{\text{train}}^i \leftarrow \left\{\boldsymbol{x}_0, \boldsymbol{x}_1^i, \boldsymbol{x}_2^i, \cdots, \boldsymbol{x}_T^i\right\}$ ▷ Generate training data based on the previous policy $\boldsymbol{p}^{i-1}(\boldsymbol{x}_t)$

Evaluate a loss function

$$\ell_{\boldsymbol{\nu}} := \frac{1}{N_{\text{path length}}} \sum_{\mathbf{x}_t \text{on sim. path}} \sum_{m=1}^{N_{eq}} \left(G_m(\mathbf{x}_t, \mathcal{N}(\mathbf{x}_t))\right)^2$$

for $k \in \{1, 2, \cdots, \texttt{len}(\boldsymbol{\nu})\}$ **do** ▷ Perform stochastic gradient descent

$$\nu_k^{'} = \nu_k - \alpha^{\text{learn}} \frac{\partial \ell(\boldsymbol{\nu})}{\partial \nu_k}$$

end for

$i \leftarrow i + 1$ ▷ Go to the next episode $i + 1$

end while

return $\nu^* \leftarrow \nu^i$ ▷ Optimal policy at convergence: $\boldsymbol{p}^*(\boldsymbol{x}_t) \approx \mathcal{N}(\boldsymbol{x}_t)$

Part 2: Uncertainty quantification based on GP surrogate models

Uncertainty quantification using the predictive mean of the GP surrogate model $\mathcal{M}_{\text{GP}|\Theta_s, y_s}$.

Input:

$\boldsymbol{p}^*(\boldsymbol{x}_t)$ (optimal policy functions), n (size of training set for the GPs), and y (QoI, e.g., the SCC).

Output:

S_i (the first-order Sobol' indices), U_i (the univariate effects) and Sh_i (the Shapley values) for the uncertain parameter ϑ_i.

while $\varepsilon_{\text{GP}|\Theta_s, y_s}^{\text{LOO}} \geq \epsilon_{\text{GP}}^{\text{LOO}}$ **do** ▷ Criterion to ensure high-quality GP surrogate model (cf. appendix B.3)

for $j \in \{1, ..., n\}$ **do** ▷ Generate a training set $\mathcal{D}_s$ for the GP

$y_j = \mathcal{M}(\boldsymbol{\vartheta}_j)$ ▷ Compute the QoI for a given combination of parameters $\boldsymbol{\vartheta}_j$ by using $\boldsymbol{p}^*(\boldsymbol{x}_t)$

end for

Fit the GP model $\mathcal{M}_{\text{GP}|\Theta_s, y_s}$ to $\mathcal{D}_s$

Compute the leave-one-out error $\epsilon_{\text{GP}|\Theta_s, y_s}^{\text{LOO}}$

$n \leftarrow n + 1$ ▷ Increase the size of the training set if necessary

end while

return $\mathcal{M}_{\text{GP}|\Theta_s, y_s}$ ▷ Accurate GP surrogate model; used to replace true model $\mathcal{M}(\cdot)$ in UQ tasks

for $i \in \{1, ..., N\}$ **do** ▷ UQ for each uncertain parameter ϑ_i

Compute the Sobol' indices S_i (cf. Eq. (50)).

Compute the univariate effects $\mathcal{U}_i$ (cf. Eq. (51)).

Compute the Shapley values Sh_i following (cf. Eq. (52)).

return $S_i, \mathcal{U}_i$ and Sh_i

end for

5 Results

This section reports the preliminary results. The results reported are for the case of the damages as presented in Eq. (5). The case of damages with tipping is still work in progress. First, we describe the parameter choices for the uncertainty quantification. Second, we briefly present the optimal policy results for three types of models: the fully deterministic model, the model with the temperature shock, and the one with the Bayesian learning over the equilibrium climate sensitivity - our benchmark model. Third, we complete the section by discussing the results of the uncertainty quantification and outlining further research steps.

5.1 Parameters for the uncertainty quantification analysis

We subjectively select uncertain parameters $\boldsymbol{\vartheta}$ as summarized in Table 1. We introduce three uncertain parameters from the economic module and three from the climate module. From the economic module, we include the pure rate of time preferences ρ, the Arrow-Patt relative risk aversion γ and the intertemporal elasticity of substitution ψ that characterize the Epstein-Zin preferences.

From the climate module, we include the initial values of the prior mean $\mu_{f,0}$ and variance $S_{f,0}$ of the Bayesian learning process over equilibrium climate sensitivity. We as well include damage parameter π_2 that is a part of the quadratic damage function.

As there is no apriori knowledge available on the distribution of each uncertain parameter ϑ_i, in line with Harenberg et al. (2019), we assume an uniform distribution with a lower $\underline{\vartheta}_i$ and upper bound $\overline{\vartheta}_i$, and each parameter ϑ_i is statistically independent, as reported in Table 1. $\vartheta_i \in \left[\underline{\vartheta}_i, \overline{\vartheta}_i\right]$ shall be plausible yet still subjectively selected to include common values in the literature.

5.2 Optimal policy

In this section, we present and briefly discuss the optimal policy results for the deterministic model, a model with the temperature shock without learning and Bayesian learning over the ECS. In the Figure 2, we see that optimal emissions are the highest for

Table 1: Parameter ranges for the uncertainty quantification analysis.

Parameter	ϑ_i^0	$\underline{\vartheta}_i$	$\overline{\vartheta}_i$	Source etc.
ρ	0.015	0.01	0.02	Stern (2008)
γ	10	5	10.	Jensen and Traeger (2014) and Cai and Lontzek (2019)
ψ	1.5	1.2	2.0	Jensen and Traeger (2014) and Cai and Lontzek (2019)
π_2	0.00236	0.002	0.008	Nordhaus (2017) and Weitzman (2012)
$\mu_{f,0}$	0.65	0.45	0.73	Roe and Baker (2007) and Folini et al. (2023)
$S_{f,0}$	0.0169	0.01	0.04	Roe and Baker (2007)

the case with learning and the lowest for the deterministic case. The intuition behind this result is that in order to learn the ECS, the agent needs to emit more carbon in the beginning.

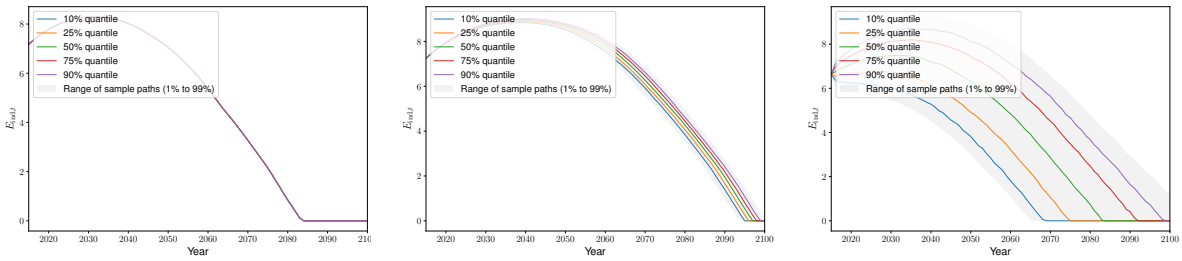

(a) Deterministic (b) Stochastic temperature (c) Bayesian learning

Figure 2: Emissions in deterministic case (left), with temperature shocks (middle), and with Bayesian learning (right).

The mean of atmospheric temperature increase in the Figure 3 is approximately the same in all the cases and comprises $2.5°C$. The variance of the temperature increase is observed to be the highest in the case of learning, as the model features two types of shocks, one to the climate feedback parameter and one to the temperature itself.

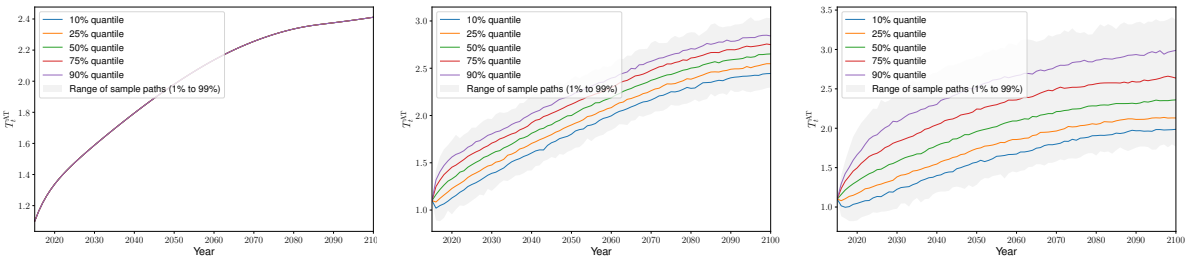

(a) Deterministic (b) Stochastic temperature (c) Bayesian learning

Figure 3: Temperature of the atmosphere in deterministic case (left), stochastic temperature (middle), and with learning (right).

Abatement level in Figure 4 as well as the value of the social cost of carbon in Figure 5 are the lowest for the deterministic case, with more abatement in place in case of a stochastic temperature and also in case of learning. This reveals the precautionary motive of the agent to increase abatement in case of uncertainty. The abatement rate, as well as the SCC in the case of stochastic temperature, is slightly higher than in the case of learning. This is due to the fact that in the case of learning, the agent does not have such a strong precautionary motive to increase abatement as in the case of purely stochastic temperature shock because more emissions help the agent to learn quicker.

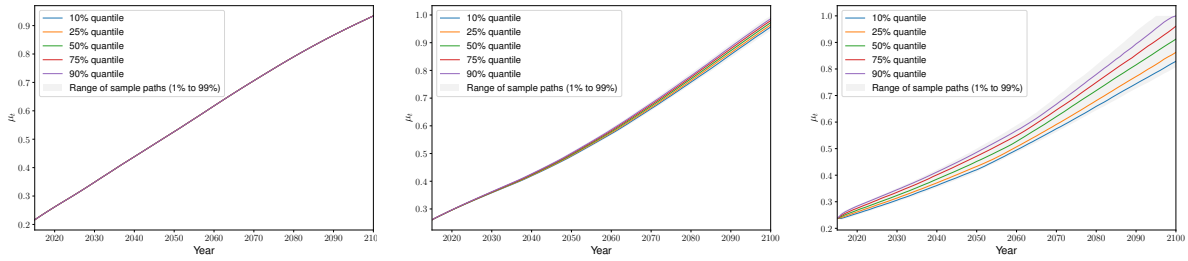

(a) Deterministic (b) Stochastic temperature (c) Bayesian learning

Figure 4: Abatement in deterministic case (left), stochastic temperature (middle), and with Bayesian learning (right).

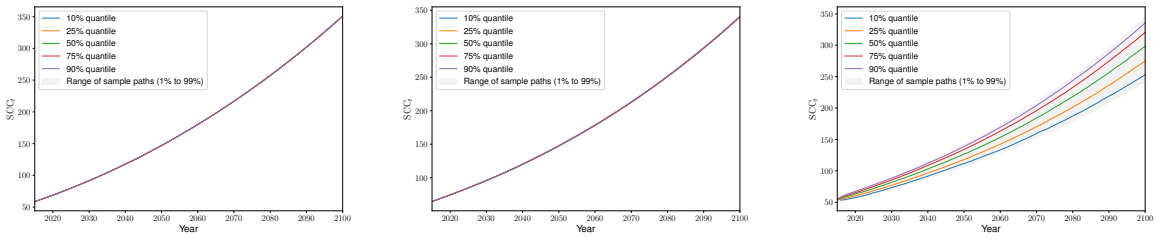

(a) Deterministic (b) Stochastic temperature (c) Bayesian learning

Figure 5: SCC in deterministic case (left), stochastic temperature (middle), and with Bayesian learning (right).

Overall the results found from the comparison of three types of models correspond to the findings in the literature, for example, Kelly and Tan (2015) and Hwang et al. (2017). However, our results are different from Jensen and Traeger (2013). They find that first, there is no change in mitigation and a slight increase in emissions in the stochastic temperature case in comparison to the deterministic case. Second, they also find there is more mitigation under the Bayesian learning case in comparison to the stochastic temperature case. The differences in results can be potentially explained by the fact that Jensen and Traeger (2013) did not use the disentangled Epstein-Zin preferences, and also, the variance of the stochastic temperature shock in their model is almost two orders of magnitude higher than in our model.

5.3 Uncertainty quantification results

The Figure 6 presents the value of Shapley indices (in blue) and Sobol indices (in green) for the impact of uncertain parameters on the value of the social cost of carbon (SCC) in years 2020, 2050, and 2100. Both indices measure the contribution of the uncertain parameters into the decomposition of the variance of the quantity of interest, in our case, the value of the SCC.

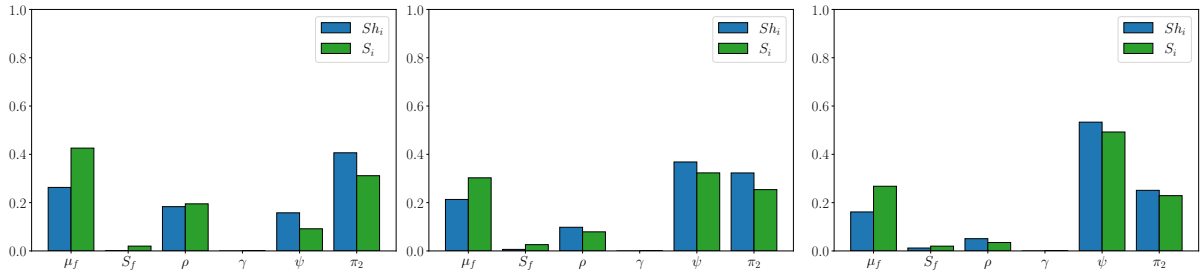

(a) 2020 (b) 2050 (c) 2100

Figure 6: Impact of the uncertain parameters on the SCC in 2020 (left), SCC in 2050 (middle), and SCC in 2100 (right) in the model with Bayesian learning.

First, we can observe that the uncertainty around the prior mean of the climate feedback parameter $\mu_{f,0}$ does get resolved with the learning over time. The impact of the prior mean on the SCC decreases by 1.5 times in 2100 in comparison to the year 2020. Second, the impacts of the damage uncertainty as well as the pure rate of time preferences, are also diminishing over time. These impacts are related, as damages reflect in the social cost of carbon through the discount rate. With time the impact of the discount rate on the SCC value drops, so the damages follow the same pattern. Third, we observe the increase in the impact of the intertemporal elasticity of substitution on the SCC value over time. The SCC value in 2100 becomes robust to other uncertain parameters, and the only thing that still impacts the change in the value is the desire to smooth consumption over time. Finally, the prior variance, as well as relative risk aversion, do not have any effect on the SCC.

In the Figure 7 and Figure 8, we can see the direction of the influence of the uncertain parameter on the absolute value of the SCC. For most of the parameters, the directions of impact correspond to the economic intuition behind it: if the prior mean of the climate feedback parameter grows, the SCC grows as well; an increase in the pure rate of time preferences reduces the SCC, growth in damages leads to respective growth in the SCC.

The only parameter that impact on the SCC is not obvious is the IES. The SCC decreases in case of an increase in the IES (decrease in desire to smooth consumption). This effect becomes even stronger for the SCC in 2100.

This is different from the findings in Jensen and Traeger (2014) and Cai and Lontzek

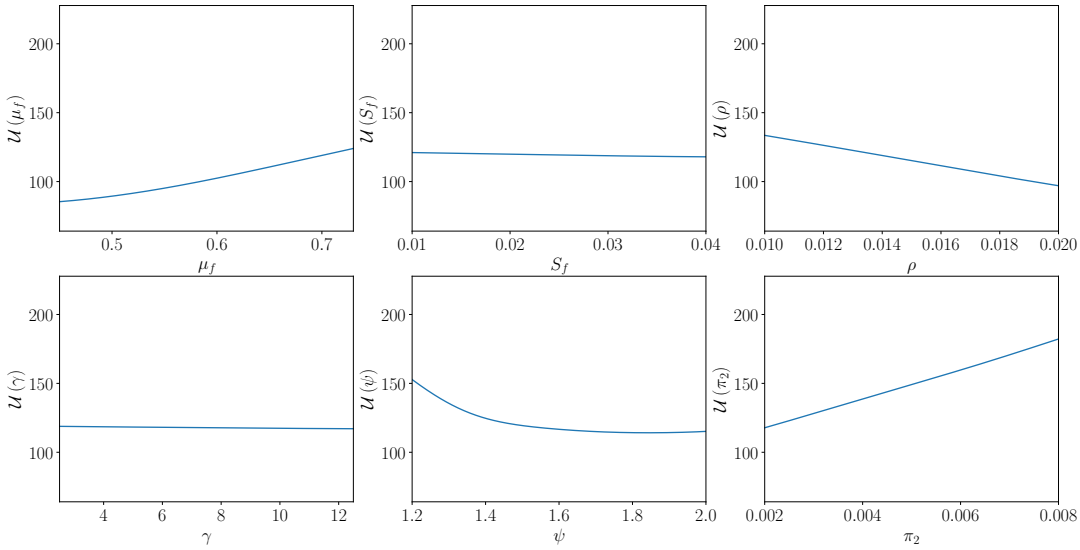

Figure 7: Univariate effects on the SCC in 2020 in a model with Bayesian learning.

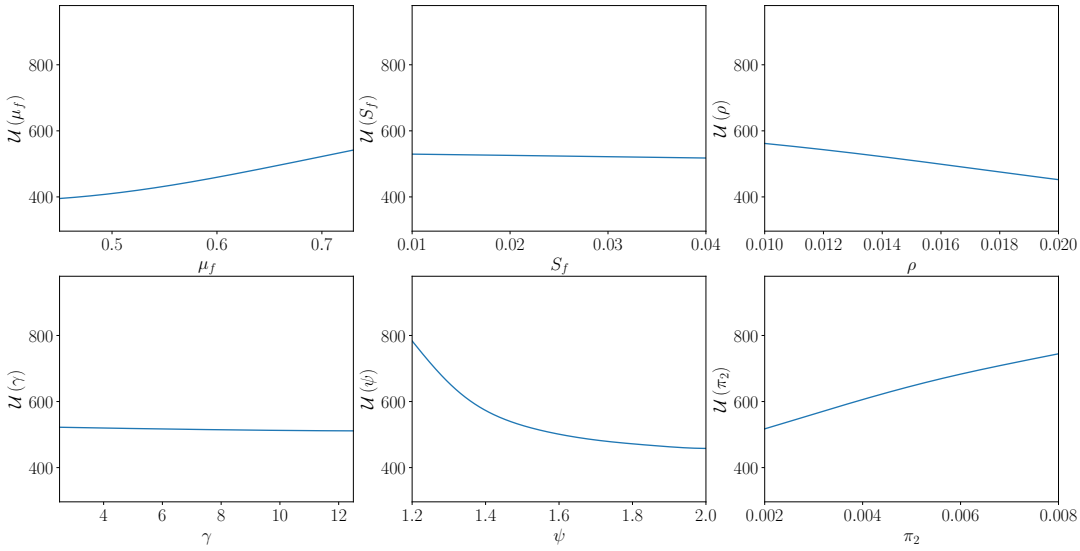

Figure 8: Univariate effects on the SCC in 2100 in a model with Bayesian learning.

(2019), which document the increase in the SCC in response to the increase in IES. However, there is an important difference between our model and the models in the studies mentioned above. Specifically, in our model, we include the temperature shocks, while in the aforementioned studies, the TFP shock is considered. It can be that TFP shock and temperature shock affect decision-making under uncertainty differently. Positive TFP shock has a counteracting first-order impact on the economy: on the one hand, it gives output; on the other hand, it is related to more emissions and, consequently, more damages. Positive temperature shock has a one-direction

first-order impact on the economy: emissions stay the same, but the net output is diminished. In both cases of shocks, the agent increases investments in capital for a precautionary motive to hedge against bad shocks. In the case of TFP shock, additional investment into mitigation helps to gain more from 'good' TFP shock. This way, the effect of positive TFP on the emission rise is being addressed by higher mitigation. In case of temperature shock, additional investment into abatement does not seem to pay off in terms of the possible gains; the precautionary motive alone may be too small to justify more abatement efforts due to little consumption smoothing desire. However, this is just one possible explanation for the results observed, and it requires further research to understand and quantify potential differences in decision-making under uncertainty coming from different sources.

6 Conclusion

The uncertainty inherent in IAMs arises from diverse origins, including modeling ambiguity, fluctuations in economic and climatic trajectories, and parametric variations, among others. This article engages in quantifying the parametric uncertainty within a stochastic IAM that i) explicitly encompasses the primary source of climatic uncertainty, i.e., the ECS, ii) encompasses the potential for the social planner to acquire knowledge about ECS through Bayesian learning, and iii) posits generic climate tipping to account for irreversible damage.

In response to these challenges, we present a novel, generic methodological approach. First, we propose a versatile, deep learning-infused solution technique for achieving a global resolution of high-dimensional, stochastic IAMs, employing Bayesian learning for ECS adaptation. Second, we employ a Gaussian process-based surrogate model to effectively propagate parametric uncertainty when assessing the social cost of carbon, achieving computational efficiency.

Our findings substantiate that the Bayesian learning process mitigates the influence of uncertain prior ECS values on the SCC and mitigates the uncertainty in the prior belief of ECS on the SCC. Simultaneously, the impact of uncertain pure rate of time preferences and the uncertainty in the damage function diminishes, while the signif-

icance of the IES for SCC gains prominence. The methodological framework that we have advanced facilitates a nuanced exploration of the intricate economic underpinnings shaping decision-making responses to uncertainty, thereby opening avenues for further research exploration.

Our novel methodology allows us to investigate further the subtle underlying economic mechanisms under the decision-making response to uncertainty, which forms the further avenue of research.

Appendix A Additional Model Details

This section introduces the complete parametrization of our annually calibrated IAM.

A.1 Exogenous variables

The law of motion for labor is given in Eq. (55) along with labor growth presented in Eq. (56):

$$L_t = L_0 + (L_\infty - L_0)\left(1 - \exp\left(-\Delta_t \delta^L t\right)\right), \tag{55}$$

$$g_t^L = \frac{\frac{dL_t}{dt}}{L_t} = \frac{\Delta_t \delta^L}{\frac{L_\infty}{L_\infty - L_0}\exp\left(\Delta_t \delta^L t\right) - 1}. \tag{56}$$

The numerical values of the parameters for the world population and its growth rate are presented in Table 2:

Calibrated parameter	Symbol	Value
Annual rate of convergence	δ^L	0.0268
World population at starting year [millions]	L_0	7403
Asymptotic world population [millions]	L_∞	11500

Table 2: Generic parameterization for the evolution of labor.

The total factor productivity evolves according to Eq. (57), and the corresponding growth rate is presented in Eq. (58):

$$A_t = A_0 \exp\left(\frac{\Delta_t g_0^A (1 - \exp(-\Delta_t \delta^A t))}{\Delta_t \delta^A}\right). \tag{57}$$

$$g_t^A = \frac{\frac{dA_t}{dt}}{A_t} = \Delta_t g_0^A \exp\left(-\Delta_t \delta^A t\right). \tag{58}$$

The parameters of the total factor productivity evolution and TFP growth rate are provided in Table 3:

Calibrated parameter	Symbol	Value
Initial growth rate for TFP per year	g_0^A	0.0217
Decline rate of TFP growth per year	δ^A	0.005
Initial level of TFP	A_0	0.010295

Table 3: Generic parametrization for the evolution of TFP.

The carbon intensity is given by:

$$\sigma_t = \sigma_0 \exp\left(\frac{\Delta_t g_0^\sigma}{\log(1+\Delta_t \delta^\sigma)}\left((1+\Delta_t\delta^\sigma)^t - 1\right)\right). \tag{59}$$

Furthermore, the parametrization for carbon intensity processes is given by Table 4:

Calibrated parameter	Symbol	Value
Initial growth of carbon intensity per year	g_0^σ	-0.0152
Decline rate of decarbonization per year	δ^σ	0.001
Initial carbon intensity (1000GtC)	σ_0	0.00009556

Table 4: Generic parameterization for the carbon intensity evolution.

Our IAM uses a backstop technology capable of mitigating the full amount of industrial emissions that enter the atmosphere. The cost of backstop technology is assumed to be initially high but could be reduced over time, which is reflected in the definition of the coefficient of the abatement cost function $\theta_{1,t}$ as defined in Eq. (60).[29]

The abatement cost is given by:

$$\theta_{1,t} = \frac{p_0^{\text{back}} \exp\left(-g^{\text{back}} t\right) 1000 \cdot \text{c2co2} \cdot \sigma_t}{\theta_2}. \tag{60}$$

The parameters for the abatement cost are presented in Table 5:

[29] The scale parameter 1000 in the equations (60) reflects the fact that we use a 1000 GtC unit of measurement; the parameter c2co2 transforms carbon intensity measured in GtC into $GtCO_2$, as the backstop price in DICE-2016 is given for $GtCO_2$ instead of GtC.

Calibrated parameter	Symbol	Value
Cost of backstop 2010 thUSD per tCO_2 2015	p_0^{back}	0.55
Initial cost decline backstop cost per year	g^{back}	0.005
Exponent of control cost function	θ_2	2.6
Transformation coefficient from C to CO_2	c2co2	3.666

Table 5: Generic parametrization for the abatement cost.

The non-industrial emissions from land use and deforestation decline over time according to Eq. (61), with parameters are presented in Table 6:

$$E_{\text{Land},t} = E_{\text{Land},0} \exp\left(-\Delta_t \delta^{\text{Land}} t\right). \tag{61}$$

Calibrated parameter	Symbol	Value
Emissions from land 2015 (1000GtC per year)	$E_{\text{Land},0}$	0.000709
Decline rate of land emissions (per year)	δ^{Land}	0.023

Table 6: Generic parametrization for the emissions from land.

The exogenous radiative forcings that result from non-CO_2 GHG are described in Eq. (62):

$$F_t^{EX} = F_0^{EX} + \frac{1}{\mathrm{T}/\Delta_t}(F_1^{EX} - F_0^{EX}) \min(t, \mathrm{T}/\Delta_t). \tag{62}$$

The parameters of the exogenous radiative forcings are given in Table 7:

Calibrated parameter	Symbol	Value
2015 forcings of non-CO_2 GHG (Wm-2)	F_0^{EX}	0.5
2100 forcings of non-CO_2 GHG (Wm-2)	F_1^{EX}	1.0
Number of years before 2100	T	85

Table 7: Generic parametrization for the exogenous forcing.

A.2 The climate model

The parameters for the laws of motion for the masses of carbon, as well as the starting values and equilibrium values, are given in Table 8. We define: $b_{21} = b_{12}\frac{M_{\text{EQ}}^{\text{AT}}}{M_{\text{EQ}}^{\text{UO}}}$, $b_{32} =$

$b_{23}\frac{M_{\text{EQ}}^{\text{UO}}}{M_{\text{EQ}}^{\text{LO}}}$.

Calibrated parameter	Symbol	Value
Carbon cycle, annual value	b_{12}	0.054
Carbon cycle, annual value	b_{23}	0.0082
Equilibrium concentration in atmosphere (1000GtC)	$M_{\text{EQ}}^{\text{AT}}$	0.607
Equilibrium concentration in upper strata (1000GtC)	$M_{\text{EQ}}^{\text{UO}}$	0.489
Equilibrium concentration in lower strata (1000GtC)	$M_{\text{EQ}}^{\text{LO}}$	1.281
Concentration in atmosphere 2015 (1000GtC)	$M_{\text{INI}}^{\text{AT}}$	0.851
Concentration in upper strata 2015 (1000GtC)	$M_{\text{INI}}^{\text{UO}}$	0.628
Concentration in lower strata 2015 (1000GtC)	$M_{\text{INI}}^{\text{LO}}$	1.323

Table 8: Generic parametrization for the mass of carbon.

The parameters and starting values of temperature evolution and Bayesian learning are given in Table 10:

Calibrated parameter	Symbol	Value
Temperature coefficient, annual value	c_1	0.137
Temperature coefficient, annual value	c_3	0.73
Temperature coefficient, annual value	c_4	0.00689
Forcings of equilibrium CO_2 doubling (Wm-2)	F_{2XCO2}	3.45
Eq temperature impact (°C per doubling CO_2)	T_{2XCO2}	3.25
Eq concentration in atmosphere (1000GtC)	$M_{\text{base}}^{\text{AT}}$	0.607
Atmospheric temp change (°C) from 1850	T_0^{AT}	1.1
Lower stratum temp change (°C) from 1850	T_0^{OC}	0.27

Table 9: Generic parametrization for the temperature.

The parameters and starting values of Bayesian learning are given in Table 10:

Calibrated parameter	Symbol	Value
Initial prior mean	$\mu_{f,0}$	0.65
Initial prior variance	$S_{f,0}$	0.0169
Upper bound for a climate feedback parameters	$\overline{f}$	0.85
Lower bound for a climate feedback parameters	$\underline{f}$	0.45
Reference temperature impact (°C per doubling CO_2)	$\overline{\Delta T}_{\text{ATX2}}^{\circ}$	1.2
Variance of temperature shock	S_{ϵ^T}	0.01

Table 10: Generic parametrization for the Bayesian learning process.

A.3 The economy

The parameters for the economic part of the model are given in Table 12.

Calibrated parameter	Symbol	Value
Capital annual depreciation rate	δ^K	0.1
Elasticity of capital	α	0.3
Damage parameter	ψ_1	20.46
Damage parameter	π_1	0.0
Damage parameter	π_2	0.00236
Tipping point variance	S_{TP}	0.01
Exponent of control cost function	θ_2	2.6
Intertemporal elasticity of substitution	ψ	1.5
Risk aversion	γ	10.
Time preferences	ρ	0.015

Table 11: Generic parameterization for the parameters of the economy.

Appendix B Implementation Details

In this section, we discuss some practical points when an IAM is mapped to the DEQN solution method.

B.1 Deep equilibrium nets for stochastic IAMs

In this Appendix, we provide a detailed procedure for mapping a stochastic, nonlinear, and non-stationary IAM onto the DEQN solution framework. The original problem, as introduced in Section 3.4 (cf. Eqs. (20) to (32))), requires some modifications to leverage the capabilities of the DEQN.

Recall that the state of the economy at time t is given by

$$\mathbf{X}_t \in \mathbb{R}^{10+N} := \left(K_t, M_t^{\mathrm{AT}}, M_t^{\mathrm{UO}}, M_t^{\mathrm{LO}}, T_t^{\mathrm{AT}}, T_t^{\mathrm{OC}}, \mu_{f,t}, S_{f,t}, TP_t, t, \boldsymbol{\vartheta}\right)^T \tag{63}$$

, where, next to the endogenous and exogenous state variables, we consider N uncertain parameters as pseudo-state variables.

Following, for instance Folini et al. (2023), we consider time t as an exogenous state to account for the non-stationary nature of the IAM, whereas all the other states

except the pseudo-states ϑ are endogenously determined. Furthermore, to ensure computational tractability, we follow Traeger (2014) and map the unbounded physical time $t \in [0, \infty)$ via the strictly monotonic transformation,

$$\tau = 1 - \exp(-\varsigma t), \tag{64}$$

into the unit interval $\tau \in (0, 1]$. To scale back from the artificial time τ to the physical time, the inverse transformation of equation (64) can be applied, that is,

$$t = -\frac{\ln(1-\tau)}{\varsigma}. \tag{65}$$

It is known that the dynamic programming problem presented in Section 3.4 would be computationally inefficient and unstable, mainly due to the capital stock that evolves significantly over time. Following Traeger (2014) among others, we normalize economic variables, capital stock, consumption, and investment, as well as the value function in the effective labor units, that is,

$$c_t := \frac{C_t}{A_t L_t}, k_t := \frac{K_t}{A_t L_t}, i_t := \frac{I_t}{A_t L_t}, v_t := \frac{V_t}{A_t L_t^{\frac{1}{1-1/\psi}}}, \tag{66}$$

where A_t represents a deterministic TFP growth trend and L_t is the global population (or labor).

Furthermore, we introduce a quantity called the effective, or growth-adjusted, discount factor,

$$\hat{\beta}_t := \exp\left(-\rho + \left(1 - \frac{1}{\psi}\right) g_t^A + g_t^L\right). \tag{67}$$

Using Eq. (66), we transform the original dynamic programming problem.

Furthermore, we also apply Eqs. (18) and (19) and also leverage the fact that $\tilde{f}_{t+1} = \mu_{f,t} + \sqrt{S_{f,t}}\epsilon^f$, where $\epsilon^f \sim \mathcal{N}\left(0, 1, \underline{\epsilon^f}, \overline{\epsilon^f}\right)$, $\underline{\epsilon^f} = \frac{\underline{f} - \mu_{f,t}}{\sqrt{S_{f,t}}}$, $\overline{\epsilon^f} = \frac{\overline{f} - \mu_{f,t}}{\sqrt{S_{f,t}}}$. For simplicity we replace $\epsilon_{T,t+1}$ from Eqs. (18) and (19) with by the short-hand notation ϵ^T. The laws of

motion for posterior mean and posterior variance can be expressed as:

$$\mu_{f,t+1} = \mu_{f,t} + \frac{\sqrt{S_{f,t}} S_{f,t} \left(\varphi_{1C} T_{\mathrm{AT},t}\right)^2}{S_{\epsilon^T} + \left(\varphi_{1C} T_{\mathrm{AT},t}\right)^2 S_{f,t}} \epsilon^f + \frac{\varphi_{1C} T_{\mathrm{AT},t} S_{f,t}}{S_{\epsilon^T} + \left(\varphi_{1C} T_{\mathrm{AT},t}\right)^2 S_{f,t}} \epsilon^T, \tag{68}$$

$$S_{f,t+1} = \frac{S_{\epsilon^T} S_{f,t}}{S_{\epsilon^T} + \left(\varphi_{1C} T_{\mathrm{AT},t}\right)^2 S_{f,t}}, \tag{69}$$

where $\epsilon^f \sim \mathcal{N}\left(0, 1, \underline{\epsilon^f}, \overline{\epsilon^f}\right)$, $\underline{\epsilon^f} = \frac{\underline{f} - \mu_{f,t}}{\sqrt{S_{f,t}}}$, $\overline{\epsilon^f} = \frac{\overline{f} - \mu_{f,t}}{\sqrt{S_{f,t}}}$ and $\epsilon^T \sim \mathcal{N}(0, S_{\epsilon^T})$.

The normalized problem reads as follows:

$$v\left(\boldsymbol{x}_t\right)^{1-1/\psi} = \max_{k_{t+1}, c_t, \mu_t} \left\{ c_t^{1-1/\psi} + \beta_t \mathbb{E}_t \left[v\left(\boldsymbol{x}_{t+1}\right)^{1-\gamma} \right]^{\frac{1-1/\psi}{1-\gamma}} \right\} \tag{70}$$

$$\text{s.t.} \quad \left(1 - \Theta\left(\mu_t\right)\right) \Omega\left(T_{\mathrm{AT},t}\right) k_t^\alpha - c_t - i_t = 0 \quad \left(\lambda_t\right) \tag{71}$$

$$\left(1 - \delta\right) k_t + i_t - \exp\left(g_t^A + g_t^L\right) k_{t+1} = 0 \quad \left(\nu_t^K\right) \tag{72}$$

$$1 - \mu_t \geq 0 \quad \perp \quad \lambda_t^\mu \geq 0 \tag{73}$$

$$\left(1 - b_{12}\right) M_{\mathrm{AT},t} + b_{21} M_{\mathrm{UO},t} + \left(1 - \mu_t\right) \sigma_t A_t L_t k_t^\alpha + E_{\mathrm{Land},t} - M_{\mathrm{AT},t+1} = 0 \quad \left(\nu_t^{\mathrm{AT}}\right) \tag{74}$$

$$b_{12} M_{\mathrm{AT},t} + \left(1 - b_{21} - b_{23}\right) M_{\mathrm{UO},t} + b_{32} M_{\mathrm{LO},t} - M_{\mathrm{UO},t+1} = 0 \quad \left(\nu_t^{\mathrm{UO}}\right) \tag{75}$$

$$b_{23} M_{\mathrm{UO},t} + \left(1 - b_{32}\right) M_{\mathrm{LO},t} - M_{\mathrm{LO},t+1} = 0 \quad \left(\nu_t^{\mathrm{LO}}\right) \tag{76}$$

$$\begin{aligned} &\left(1 - c_1 c_3 - \varphi_{1C}\right) T_{\mathrm{AT},t} + c_1 c_3 T_{\mathrm{OC},t} + c_1 \left(F_{2\mathrm{xco2}} \log_2 \left(\frac{M_{\mathrm{AT},t}}{M_{\mathrm{AT}}^*} \right) + F_{\mathrm{EX},t} \right) \\ &\quad + \varphi_{1C} T_{\mathrm{AT},t} \mu_{f,t} + \varphi_{1C} T_{\mathrm{AT},t} \sqrt{S_{f,t}} \epsilon^f + \epsilon^T - T_{\mathrm{AT},t+1} = 0 \quad \left(\eta_{t+1}^{\mathrm{AT}}\right), \\ &\quad \text{where } \epsilon^f \sim \mathcal{N}\left(0, 1, \underline{\epsilon^f}, \overline{\epsilon^f}\right), \epsilon^T \sim \mathcal{N}(0, S_{\epsilon^T}) \end{aligned} \tag{77}$$

$$c_4 T_{\mathrm{AT},t} + \left(1 - c_4\right) T_{\mathrm{OC},t} - T_{\mathrm{OC},t+1} = 0 \quad \left(\eta_t^{\mathrm{OC}}\right) \tag{78}$$

$$\begin{aligned} &\mu_{f,t} + \frac{\sqrt{S_{f,t}} S_{f,t} \left(\varphi_{1C} T_{\mathrm{AT},t}\right)^2}{S_{\epsilon^T} + \left(\varphi_{1C} T_{\mathrm{AT},t}\right)^2 S_{f,t}} \epsilon^f + \frac{\varphi_{1C} T_{\mathrm{AT},t} S_{f,t}}{S_{\epsilon^T} + \left(\varphi_{1C} T_{\mathrm{AT},t}\right)^2 S_{f,t}} \epsilon^T - \mu_{f,t+1} = 0 \quad \left(\lambda_{t+1}^{\mu_f}\right) \\ &\quad \text{where } \epsilon^f \sim \mathcal{N}\left(0, 1, \underline{\epsilon^f}, \overline{\epsilon^f}\right), \epsilon^T \sim \mathcal{N}(0, S_{\epsilon^T}) \end{aligned} \tag{79}$$

$$\frac{S_{\epsilon^T} S_{f,t}}{S_{\epsilon^T} + \left(\varphi_{1C} T_{\mathrm{AT},t}\right)^2 S_{f,t}} - S_{f,t+1} = 0 \quad \left(\lambda_t^{S_f}\right) \tag{80}$$

where the Lagrange multipliers we will employ below have been added in parentheses

for completeness. In Eq. (73), the symbol $\perp$ indicates complementary slackness. Note also that the Lagrangian multipliers η_{t+1}^{AT} in Eq. (77) and $\lambda_{t+1}^{\mu_f}$ in Eq. (79) are stochastic due to the uncertain shocks ϵ^f, ϵ^T.

The policy function $\mathbf{p}$ we intend to approximate with the aid of deep neural networks is given by

$$\mathcal{N}(\mathbf{x}_t) \in \mathbb{R}^{14} := \left(c_t, i_t, v_t, \mu_t, \lambda_t, \eta_t^K, \lambda_t^\mu, \nu_t^{\mathrm{AT}}, \nu_t^{\mathrm{UO}}, \nu_t^{\mathrm{LO}}, \eta_{t+1}^{\mathrm{AT}}\eta_t^{\mathrm{OC}}, \lambda_{t+1}^{\mu_f}, \lambda_t^{S_f}\right), \tag{81}$$

and consists of the choice variables (c_t, i_t, μ_t)[30] as well as the Lagrange and KKT multipliers.

Next, we derive the first-order conditions to form a loss function for the IAM model that is suitable for DEQNs (cf. Eq. (36)).

We derive the following first-order conditions in effective labor units.

$$\frac{\partial v_t}{\partial k_{t+1}} = \left(1 - \frac{1}{\psi}\right)\beta_t \mathbb{E}_t\left[v_{t+1}^{1-\gamma}\right]^{\frac{\gamma-1/\psi}{1-\gamma}} \mathbb{E}_t\left[v_{t+1}^{-\gamma} v_{k,t+1}\right] - \lambda_t \exp\left(g_t^A + g_t^L\right) = 0 \tag{82}$$

$$\frac{\partial v_t}{\partial c_t} = \left(1 - \frac{1}{\psi}\right) c_t^{-\frac{1}{\psi}} - \lambda_t = 0 \tag{83}$$

$$\frac{\partial v_t}{\partial \mu_t} = \lambda_t \Theta'(\mu_t)\,\Omega_t\,(T_{\mathrm{AT},t})\,k_t^\alpha + \lambda_t^\mu + \nu_t^{\mathrm{AT}}\sigma_t A_t L_t k_t^\alpha = 0 \tag{84}$$

$$\frac{\partial v_t}{\partial M_{\mathrm{AT},t+1}} = \left(1 - \frac{1}{\psi}\right)\beta_t \mathbb{E}_t\left[v_{t+1}^{1-\gamma}\right]^{\frac{\gamma-1/\psi}{1-\gamma}} \mathbb{E}_t\left[v_{t+1}^{-\gamma} v_{M_{\mathrm{AT}},t+1}\right] - \nu_t^{\mathrm{AT}} = 0 \tag{85}$$

$$\frac{\partial v_t}{\partial M_{\mathrm{UO},t+1}} = \left(1 - \frac{1}{\psi}\right)\beta_t \mathbb{E}_t\left[v_{t+1}^{1-\gamma}\right]^{\frac{\gamma-1/\psi}{1-\gamma}} \mathbb{E}_t\left[v_{t+1}^{-\gamma} v_{M_{\mathrm{UO}},t+1}\right] - \nu_t^{\mathrm{UO}} = 0 \tag{86}$$

$$\frac{\partial v_t}{\partial M_{\mathrm{LO},t+1}} = \left(1 - \frac{1}{\psi}\right)\beta_t \mathbb{E}_t\left[v_{t+1}^{1-\gamma}\right]^{\frac{\gamma-1/\psi}{1-\gamma}} \mathbb{E}_t\left[v_{t+1}^{-\gamma} v_{M_{\mathrm{LO}},t+1}\right] - \nu_t^{\mathrm{LO}} = 0 \tag{87}$$

$$\begin{aligned}\frac{\partial v_t}{\partial T_{\mathrm{AT},t+1}} &= \left(1 - \frac{1}{\psi}\right)\beta_t \mathbb{E}_t\left[v_{t+1}^{1-\gamma}\right]^{\frac{\gamma-1/\psi}{1-\gamma}} \mathbb{E}_t\left[v_{t+1}^{-\gamma} v_{T_{\mathrm{AT}},t+1}\right] \\ &- \int_{-\infty}^{+\infty}\int_{\underline{\epsilon^f}}^{\overline{\epsilon^f}} \eta_{t+1}^{\mathrm{AT}}(\epsilon^f, \epsilon^T)\mathrm{pdf}(\epsilon^f)d\epsilon^f\,\mathrm{pdf}(\epsilon^T)d\epsilon^T = 0\end{aligned} \tag{88}$$

$$\frac{\partial v_t}{\partial T_{\mathrm{OC},t+1}} = \left(1 - \frac{1}{\psi}\right)\beta_t \mathbb{E}_t\left[v_{t+1}^{1-\gamma}\right]^{\frac{\gamma-1/\psi}{1-\gamma}} \mathbb{E}_t\left[v_{t+1}^{-\gamma} v_{T_{\mathrm{OC}},t+1}\right] - \eta_t^{\mathrm{OC}} = 0 \tag{89}$$

[30] We keep the first-order conditions with respect to k_{t+1} and i_t. In practical applications, the performance of neural networks can, as in our case, often benefit from redundant information (see, e.g., Azinovic et al. (2022) for more details).

$$\frac{\partial v_t}{\partial \mu_{f,t+1}} = \left(1 - \frac{1}{\psi}\right) \beta_t \mathbb{E}_t \left[v_{t+1}^{1-\gamma}\right]^{\frac{\gamma-1/\psi}{1-\gamma}} \mathbb{E}_t \left[v_{t+1}^{-\gamma} v_{\mu_f,t+1}\right]$$
$$- \int_{-\infty}^{+\infty} \int_{\underline{\epsilon^f}}^{\overline{\epsilon^f}} \lambda_{t+1}^{\mu_f}(\epsilon^f, \epsilon^T) \text{pdf}(\epsilon^f) d\epsilon^f \text{pdf}(\epsilon^T) d\epsilon^T = 0 \tag{90}$$

$$\frac{\partial v_t}{\partial S_{f,t+1}} = \left(1 - \frac{1}{\psi}\right) \beta_t \mathbb{E}_t \left[v_{t+1}^{1-\gamma}\right]^{\frac{\gamma-1/\psi}{1-\gamma}} \mathbb{E}_t \left[v_{t+1}^{-\gamma} v_{S_f,t+1}\right] - \lambda_t^{S_f} = 0 \tag{91}$$

At the equilibrium, the following envelop theorem conditions hold

$$v_{k,t} = \frac{\partial v_t}{\partial k_t} = \lambda_t \frac{\partial k_{t+1}}{\partial k_t} + \nu_t^{\text{AT}} \frac{\partial M_{\text{AT},t+1}}{\partial k_t}$$
$$\Leftrightarrow \left(1 - \frac{1}{\psi}\right) v_t^{-1/\psi} v_{k,t} = \lambda_t \left\{\left(1 - \Theta\left(\mu_t\right)\right) \Omega\left(T_{\text{AT},t}\right) \alpha k_t^{\alpha-1} + (1 - \delta)\right\}$$
$$+ \nu_t^{\text{AT}} \left(1 - \mu_t\right) \sigma_t A_t L_t \alpha k_t^{\alpha-1} \tag{92}$$

$$v_{M_{\text{AT}},t} = \frac{\partial v_t}{\partial M_{\text{AT},t}} = \nu_t^{\text{AT}} \frac{\partial M_{\text{AT},t+1}}{\partial M_{\text{AT},t}} + \nu_t^{\text{UO}} \frac{\partial M_{\text{UO},t+1}}{\partial M_{\text{AT},t}} + \eta_{t+1}^{\text{AT}} \frac{\partial T_{\text{AT},t+1}}{\partial M_{\text{AT},t}}$$
$$\Leftrightarrow \left(1 - \frac{1}{\psi}\right) v_t^{-1/\psi} v_{M_{\text{AT}},t} = \nu_t^{\text{AT}} \left(1 - b_{12}\right) + \nu_t^{\text{UO}} b_{12} +$$
$$c_1 F_{2\text{xco2}} \frac{1}{\log 2 M_{\text{AT},t}} \int_{-\infty}^{+\infty} \int_{\underline{\epsilon^f}}^{\overline{\epsilon^f}} \eta_{t+1}^{\text{AT}}(\epsilon^f, \epsilon^T) \text{pdf}(\epsilon^f) d\epsilon^f \text{pdf}(\epsilon^T) d\epsilon^T \tag{93}$$

$$v_{M_{\text{UO}},t} = \frac{\partial v_t}{\partial M_{\text{UO},t}} = \nu_t^{\text{AT}} \frac{\partial M_{\text{AT},t+1}}{\partial M_{\text{UO},t}} + \nu_t^{\text{UO}} \frac{\partial M_{\text{UO},t+1}}{\partial M_{\text{UO},t}} + \nu_t^{\text{LO}} \frac{\partial M_{\text{LO},t+1}}{\partial M_{\text{UO},t}}$$
$$\Leftrightarrow \left(1 - \frac{1}{\psi}\right) v_t^{-1/\psi} v_{M_{\text{UO}},t} = \nu_t^{\text{AT}} b_{21} + \nu_t^{\text{UO}} \left(1 - b_{21} - b_{23}\right) + \nu_t^{\text{LO}} b_{23} \tag{94}$$

$$v_{M_{\text{LO}},t} = \frac{\partial v_t}{\partial M_{\text{LO},t}} = \nu_t^{\text{UO}} \frac{\partial M_{\text{UO},t+1}}{\partial M_{\text{LO},t}} + \nu_t^{\text{LO}} \frac{\partial M_{\text{LO},t+1}}{\partial M_{\text{LO},t}}$$
$$\Leftrightarrow \left(1 - \frac{1}{\psi}\right) v_t^{-1/\psi} v_{M_{\text{LO}},t} = \nu_t^{\text{UO}} b_{32} + \nu_t^{\text{LO}} \left(1 - b_{32}\right) \tag{95}$$

$$v_{T_{\text{AT}},t} = \frac{\partial v_t}{\partial T_{\text{AT},t}} = \lambda_t \frac{\partial k_{t+1}}{\partial T_{\text{AT},t}} + \eta_{t+1}^{\text{AT}} \frac{\partial T_{\text{AT},t+1}}{\partial T_{\text{AT},t}} + \eta_t^{\text{OC}} \frac{\partial T_{\text{OC},t+1}}{\partial T_{\text{AT},t}} + \lambda_{t+1}^{\mu_f} \frac{\partial \mu_{f,t+1}}{\partial T_{\text{AT},t}} + \lambda_t^{S_f} \frac{\partial S_{f,t+1}}{\partial T_{\text{AT},t}}$$
$$\Leftrightarrow \left(1 - \frac{1}{\psi}\right) v_t^{-1/\psi} v_{T_{\text{AT}},t} = \lambda_t \left(1 - \Theta\left(\mu_t\right)\right) \Omega'\left(T_{\text{AT},t}\right) k_t^{\alpha}$$
$$+ \int_{-\infty}^{+\infty} \int_{\underline{\epsilon^f}}^{\overline{\epsilon^f}} \eta_{t+1}^{\text{AT}}\left(\epsilon^f, \epsilon^T\right) \left(\left(1 - c_1 c_3 - \varphi_{1C}\right) + \varphi_{1C} \mu_{f,t} + \varphi_{1C} \sqrt{S_{f,t}} \epsilon^f\right) \text{pdf}(\epsilon^f) d\epsilon^f \text{pdf}(\epsilon^T) d\epsilon^T$$
$$+ \eta_t^{\text{OC}} c_4 +$$

$$\int_{-\infty}^{+\infty}\int_{\underline{\epsilon^f}}^{\overline{\epsilon^f}}\lambda_{t+1}^{\mu_f}\left(\epsilon^f,\epsilon^T\right)\frac{2S_{f,t}^{3/2}\varphi_{1C}^2T_{AT,t}S_{\epsilon^T}\epsilon^f+\varphi_{1C}S_{f,t}S_{\epsilon^T}\epsilon^T-\varphi_{1C}^3T_{AT,t}^2S_{f,t}^2\epsilon^T}{\left(S_{\epsilon^T}+\left(\varphi_{1C}T_{AT,t}\right)^2S_{f,t}\right)^2}\text{pdf}(\epsilon^f)d\epsilon^f\text{pdf}(\epsilon^T)d\epsilon^T$$

$$-\lambda_t^{S_f}\frac{2S_{\epsilon^T}\varphi_{1C}^2T_{AT,t}S_{f,t}^2}{\left(S_{\epsilon^T}+\left(\varphi_{1C}T_{AT,t}\right)^2S_{f,t}\right)^2} \tag{96}$$

$$v_{T_{OC},t}=\frac{\partial v_t}{\partial T_{OC,t}}=\eta_{t+1}^{AT}\frac{\partial T_{AT,t+1}}{\partial T_{OC,t}}+\eta_t^{OC}\frac{\partial T_{OC,t+1}}{\partial T_{OC,t}}$$

$$\Leftrightarrow\left(1-\frac{1}{\psi}\right)v_t^{-1/\psi}v_{T_{OC},t}=c_1c_3\int_{-\infty}^{+\infty}\int_{\underline{\epsilon^f}}^{\overline{\epsilon^f}}\eta_{t+1}^{AT}(\epsilon^f,\epsilon^T)\text{pdf}(\epsilon^f)d\epsilon^f\text{pdf}(\epsilon^T)d\epsilon^T+\eta_t^{OC}(1-c_4) \tag{97}$$

$$v_{\mu_f,t}=\frac{\partial v_t}{\partial\mu_{f,t}}=\eta_{t+1}^{AT}\frac{\partial T_{AT,t+1}}{\partial\mu_{f,t}}+\lambda_{t+1}^{\mu_f}\frac{\partial\mu_{f,t+1}}{\partial\mu_{f,t}}$$

$$\Leftrightarrow\left(1-\frac{1}{\psi}\right)v_t^{-1/\psi}v_{\mu_{f,t}}=\varphi_{1C}T_{AT,t}\int_{-\infty}^{+\infty}\int_{\underline{\epsilon^f}}^{\overline{\epsilon^f}}\eta_{t+1}^{AT}(\epsilon^f,\epsilon^T)\text{pdf}(\epsilon^f)d\epsilon^f\text{pdf}(\epsilon^T)d\epsilon^T+$$

$$\int_{-\infty}^{+\infty}\int_{\underline{\epsilon^f}}^{\overline{\epsilon^f}}\lambda_{t+1}^{\mu_f}(\epsilon^f,\epsilon^T)\text{pdf}(\epsilon^f)d\epsilon^f\text{pdf}(\epsilon^T)d\epsilon^T \tag{98}$$

$$v_{S_f,t}=\frac{\partial v_t}{\partial S_{f,t}}=\eta_{t+1}^{AT}\frac{\partial T_{AT,t+1}}{\partial S_{f,t}}+\lambda_{t+1}^{\mu_f}\frac{\partial\mu_{f,t+1}}{\partial S_{f,t}}+\lambda_t^{S_f}\frac{\partial S_{f,t+1}}{\partial S_{f,t}}$$

$$\Leftrightarrow\left(1-\frac{1}{\psi}\right)v_t^{-1/\psi}v_{S_{f,t}}=\int_{-\infty}^{+\infty}\int_{\underline{\epsilon^f}}^{\overline{\epsilon^f}}\eta_{t+1}^{AT}(\epsilon^f,\epsilon^T)\frac{1}{2}\varphi_{1C}T_{AT,t}\sqrt{S_{f,t}}\epsilon^f\text{pdf}(\epsilon^f)d\epsilon^f\text{pdf}(\epsilon^T)d\epsilon^T$$

$$+\int_{-\infty}^{+\infty}\int_{\underline{\epsilon^f}}^{\overline{\epsilon^f}}\lambda_{t+1}^{\mu_f}(\epsilon^f,\epsilon^T)$$

$$\frac{\frac{3}{2}\sqrt{S_{f,t}}\left(\varphi_{1C}T_{AT,t}\right)^2\epsilon^fS_{\epsilon^T}+\frac{1}{2}S_{f,t}^{3/2}\left(\varphi_{1C}T_{AT,t}\right)^4\epsilon^f+\varphi_{1C}T_{AT,t}S_{\epsilon^T}\epsilon^T}{\left(S_{\epsilon^T}+\left(\varphi_{1C}T_{AT,t}\right)^2S_{f,t}\right)^2}\text{pdf}(\epsilon^f)d\epsilon^f\text{pdf}(\epsilon^T)d\epsilon^T$$

$$+\lambda_t^{S_f}\frac{S_{\epsilon^T}^2}{\left(S_{\epsilon^T}+\left(\varphi_{1C}T_{AT,t}\right)^2S_{f,t}\right)^2} \tag{99}$$

Finally, the following optimality condition holds:

$$v_t^{1-1/\psi}=c_t^{1-1/\psi}+\beta_t\mathbb{E}_t\left[v_{t+1}^{1-\gamma}\right]^{\frac{1-1/\psi}{1-\gamma}}, \tag{100}$$

as well as budget constraint, that is,

$$(1 - \Theta(\mu_t))\,\Omega(T_{\mathrm{AT},t})\,k_t^{\alpha} - c_t - i_t = 0. \tag{101}$$

We replace the KKT condition in Eq. (73) with the Fischer-Burmeister function (see, e.g., Maliar et al. (2021), and references therein) and directly embed it in the system of non-linear equilibrium conditions:

$$\Psi^{\mathrm{FB}}\left(\lambda_t^{\mu}, 1 - \mu_t\right) = \lambda_t^{\mu} + (1 - \mu_t) - \sqrt{\lambda_t^{\mu^2} + (1 - \mu_t)^2}, \tag{102}$$

where from Eq. (84), we define λ_t^{μ} such that

$$\lambda_t^{\mu} \equiv -\lambda_t \Theta'(\mu_t)\,\Omega(T_{\mathrm{AT},t})\,k_t^{\alpha} - \nu_t^{\mathrm{AT}} \sigma_t A_t L_t k_t^{\alpha}. \tag{103}$$

One feature one faces with working with first-order conditions of an IAM is that one needs to compute them not only with respect to the economic choice variables such as μ_t and c_t, but also with respect to the climate variables, even though they are not choice variables. The reason for this is that one needs to assess the marginal effects of the change in choice variables that propagates through the climate system. Those effects cannot be computed analytically here, which is why we need Lagrange multipliers associated with every single climate equation (cf. Eqs. (85) to (89)) to estimate the shadow price of a marginal change in a respective constraint.

Using all the above definitions, the eleven individual components that enter the loss function amendable for the DEQN algorithm read as

$$l_1 := c_t^{1-1/\psi} + \beta_t \mathbb{E}_t\left[v_{t+1}^{1-\gamma}\right]^{\frac{1-1/\psi}{1-\gamma}} - v_t^{1-1/\psi} \tag{104}$$

$$l_2 := (1 - \Theta(\mu_t))\,\Omega(T_{\mathrm{AT},t})\,k_t^{\alpha} - c_t - i_t \tag{105}$$

$$l_3 := \lambda_t^{\mu} + (1 - \mu_t) - \sqrt{\lambda_t^{\mu^2} + (1 - \mu_t)^2} \tag{106}$$

$$l_4 := \lambda_t \exp\left(g_t^A + g_t^L\right) - \left(1 - \frac{1}{\psi}\right)\beta_t \mathbb{E}_t\left[v_{t+1}^{1-\gamma}\right]^{\frac{\gamma-1/\psi}{1-\gamma}} \mathbb{E}_t\left[v_{t+1}^{-\gamma} v_{k,t+1}\right] \tag{107}$$

$$l_5 := \nu_t^{\mathrm{AT}} - \left(1 - \frac{1}{\psi}\right)\beta_t \mathbb{E}_t\left[v_{t+1}^{1-\gamma}\right]^{\frac{\gamma-1/\psi}{1-\gamma}} \mathbb{E}_t\left[v_{t+1}^{-\gamma} v_{M_{\mathrm{AT}},t+1}\right] \tag{108}$$

$$l_6 := \nu_t^{\mathrm{UO}} - \left(1 - \frac{1}{\psi}\right) \beta_t \mathbb{E}_t \left[v_{t+1}^{1-\gamma}\right]^{\frac{\gamma-1/\psi}{1-\gamma}} \mathbb{E}_t \left[v_{t+1}^{\gamma} v_{M_{\mathrm{UO}},t+1}\right] \tag{109}$$

$$l_7 := \nu_t^{\mathrm{LO}} - \left(1 - \frac{1}{\psi}\right) \beta_t \mathbb{E}_t \left[v_{t+1}^{1\gamma}\right]^{\frac{\gamma-1/\psi}{1\gamma}} \mathbb{E}_t \left[v_{t+1}^{\gamma} v_{M_{\mathrm{LO}},t+1}\right] \tag{110}$$

$$\begin{aligned} l_8 := & \int_{-\infty}^{+\infty} \int_{\underline{\epsilon^f}}^{\overline{\epsilon^f}} \eta_{t+1}^{\mathrm{AT}}(\epsilon^f, \epsilon^T) \mathrm{pdf}(\epsilon^f) d\epsilon^f \mathrm{pdf}(\epsilon^T) d\epsilon^T \\ & - \left(1 - \frac{1}{\psi}\right) \beta_t \mathbb{E}_t \left[v_{t+1}^{1-\gamma}\right]^{\frac{\gamma-1/\psi}{1-\gamma}} \mathbb{E}_t \left[v_{t+1}^{-\gamma} v_{T_{\mathrm{AT}},t+1}\right] \end{aligned} \tag{111}$$

$$l_9 := \eta_t^{\mathrm{OC}} - \left(1 - \frac{1}{\psi}\right) \beta_t \mathbb{E}_t \left[v_{t+1}^{1\gamma}\right]^{\frac{\gamma-1/\psi}{1-\gamma}} \mathbb{E}_t \left[v_{t+1}^{-\gamma} v_{T_{\mathrm{OC}},t+1}\right] \tag{112}$$

$$\begin{aligned} l_{10} := & \int_{-\infty}^{+\infty} \int_{\underline{\epsilon^f}}^{\overline{\epsilon^f}} \lambda_{t+1}^{\mu_f}(\epsilon^f, \epsilon^T) \mathrm{pdf}(\epsilon^f) d\epsilon^f \mathrm{pdf}(\epsilon^T) d\epsilon^T \\ & - \left(1 - \frac{1}{\psi}\right) \beta_t \mathbb{E}_t \left[v_{t+1}^{1-\gamma}\right]^{\frac{\gamma-1/\psi}{1-\gamma}} \mathbb{E}_t \left[v_{t+1}^{-\gamma} v_{\mu_f,t+1}\right] \end{aligned} \tag{113}$$

$$l_{11} := \lambda_t^{S_f} - \left(1 - \frac{1}{\psi}\right) \beta_t \mathbb{E}_t \left[v_{t+1}^{1-\gamma}\right]^{\frac{\gamma-1/\psi}{1-\gamma}} \mathbb{E}_t \left[v_{t+1}^{-\gamma} v_{S_f,t+1}\right] \tag{114}$$

and result in the total loss function given by

$$\ell_{\boldsymbol{\nu}} := \frac{1}{N_{\text{path length}}} \sum_{\mathbf{x}_t \text{on sim. path}} \sum_{m=1}^{N_{\mathrm{eq}}=11} \left(l_m(\mathbf{x}_t, \boldsymbol{\mathcal{N}}(\mathbf{x}_t))\right)^2 . \tag{115}$$

The final ingredient we need for the DEQN algorithm is the evolution of the state $\mathbf{x}_t$ one period forward such that the loss function (115) can be evaluated along a simulated path. In our application, $\mathbf{x}_{t+1}$ is given by

$$\mathbf{x}_{t+1} = \left(k_{t+1}, M_{t+1}^{\mathrm{AT}}, M_{t+1}^{\mathrm{UO}}, M_{t+1}^{\mathrm{LO}}, T_{t+1}^{\mathrm{AT}}, T_{t+1}^{\mathrm{OC}}, \mu_{f,t+1}, S_{f,t+1}, t+1, \boldsymbol{\vartheta}\right)^T , \tag{116}$$

where k_{t+1} is updated through the law of motion using a choice variable from the policy function Eq. (81) and the climate variables $M_{t+1}^{\mathrm{AT}}, M_{t+1}^{\mathrm{UO}}, M_{t+1}^{\mathrm{LO}}, T_{t+1}^{\mathrm{AT}}$, and T_{t+1}^{OC} can be updated via Eqs. (74) to (80), whereas time t is simply incremented by one unit, and the pseudo-states $\boldsymbol{\vartheta}$ are re-sampled from their distribution at every iteration step.

B.2 Numerical integration

For reasons of numerical tractability, we replace $\tilde{f}_{t+1} = \mu_{f,t} + \sqrt{S_{f,t}}\epsilon^f$, where $\epsilon^f \sim \mathcal{N}\left(0, 1, \underline{\epsilon^f}, \overline{\epsilon^f}\right)$, $\underline{\epsilon^f} = \frac{\underline{f} - \mu_{f,t}}{\sqrt{S_{f,t}}}$, $\overline{\epsilon^f} = \frac{\overline{f} - \mu_{f,t}}{\sqrt{S_{f,t}}}$. We replace $\epsilon_{T,t+1}$ from Eqs. (18) and (19) with the short-hand notation ϵ^T. Taking these notational changes into account, we have to approximate the following integral numerically:

$$\int_{-\infty}^{+\infty} \int_{\underline{\epsilon^f}}^{\overline{\epsilon^f}} \left(\varphi_{1C} T_{\mathrm{AT},t} \sqrt{S_{f,t}} \epsilon^f + \epsilon^T\right) \mathrm{pdf}(\epsilon^f) d\epsilon^f \, \mathrm{pdf}(\epsilon^T) d\epsilon^T \tag{117}$$

where $\mathrm{pdf}(\epsilon^f) = \frac{K}{\sqrt{2\pi}} \exp\left(-\frac{(\epsilon^f)^2}{2}\right)$, $K = \left(\mathrm{cdf}(\overline{\epsilon^f}) - \mathrm{cdf}(\underline{\epsilon^f})\right)^{-1}$, and $\mathrm{pdf}(\epsilon^T) = \frac{1}{\sqrt{2\pi S_{\epsilon_T}}} \exp\left(-\frac{(\epsilon^T)^2}{2S_{\epsilon_T}}\right)$. To apply Gauss-Hermite quadrature, we need to make a change of notation by replacing:

$$x = \frac{\epsilon^T}{\sqrt{2S_{\epsilon_T}}} \Rightarrow \epsilon^T = \sqrt{2S_{\epsilon_T}} x. \tag{118}$$

Thus we get:

$$\int_{-\infty}^{+\infty} \int_{\underline{\epsilon^f}}^{\overline{\epsilon^f}} \left(\varphi_{1C} T_{\mathrm{AT},t} \sqrt{S_{f,t}} \epsilon^f + \sqrt{2S_{\epsilon_T}} x\right) \frac{K}{\sqrt{2\pi}} \exp\left(-\frac{(\epsilon^f)^2}{2}\right) d\epsilon^f \frac{1}{\sqrt{\pi}} \exp(-x^2) dx. \tag{119}$$

With the change of variables necessary for the Gauss-Legendre quadrature, we get:

$$\sum_{i=1}^{n} \frac{w_i}{\sqrt{\pi}} \sum_{j=1}^{m} v_j \left(\varphi_{1C} T_{\mathrm{AT},t} \sqrt{S_{f,t}} \left(y_j \frac{\overline{\epsilon^f} - \underline{\epsilon^f}}{2} + \frac{\overline{\epsilon^f} + \underline{\epsilon^f}}{2}\right) + \sqrt{2S_{\epsilon_T}} x_i\right) \frac{\overline{\epsilon^f} - \underline{\epsilon^f}}{2} \frac{K}{\sqrt{2\pi}} \exp\left(-\frac{\left(y_j \frac{\overline{\epsilon^f} - \underline{\epsilon^f}}{2} + \frac{\overline{\epsilon^f} + \underline{\epsilon^f}}{2}\right)^2}{2}\right) \tag{120}$$

where w_i are Gauss-Hermite weights, x_i - Gauss-Hermite nodes, v_j are Gauss-Legendre weights, y_j - Gauss-Legendre nodes.

B.3 Error statistics

Table 12 provides detailed error statistics for the model with learning and pseudo-states at convergence. All other models presented in the article reach a similar level of accuracy.

Stats.	l_1	l_2	l_3	l_4	l_5	l_6	l_7	l_8	l_9	l_{10}	l_{11}
mean	$7.43e-4$	$3.00e-3$	$7.48e-5$	$6.06e-3$	$6.69e-4$	$4.54e-4$	$2.92e-4$	$1.44e-3$	$2.55e-3$	$9.88e-4$	$3.78e-4$
std	$1.05e-3$	$6.19e-3$	$2.34e-1$	$1.04e-2$	$7.18e-4$	$5.34e-4$	$5.02e-4$	$1.34e-3$	$4.76e-3$	$1.90e-3$	$5.18e-4$
min	$< 1.e-9$	$< 1.e-9$	$< 1.e-9$	$< 1.e-9$	$< 1.e-9$	$< 1.e-9$	$< 1.e-9$	$1.86e-9$	$< 1.e-9$	$< 1.e-9$	$< 1.e-9$
0.1%	$7.15e-7$	$1.07e-6$	$< 1.e-9$	$1.84e-6$	$5.96e-7$	$4.76e-7$	$2.68e-7$	$1.00e-6$	$1.39e-6$	$9.53e-7$	$3.27e-7$
25%	$1.84e-4$	$2.99e-4$	$< 1.e-9$	$5.14e-4$	$1.70e-4$	$1.27e-4$	$7.01e-5$	$2.77e-4$	$3.66e-4$	$2.52e-4$	$8.68e-5$
50%	$4.18e-4$	$9.15e-4$	$2.3e-10$	$1.67e-3$	$4.21e-4$	$2.95e-4$	$1.58e-4$	$6.78e-4$	$9.55e-4$	$5.97e-4$	$2.02e-4$
75%	$8.81e-4$	$3.08e-3$	$1.86e-9$	$5.99e-3$	$9.18e-4$	$6.02e-4$	$3.20e-4$	$1.43e-3$	$2.69e-3$	$1.28e-3$	$4.39e-4$
99.9%	$1.12e-2$	$6.75e-2$	$2.20e-3$	$7.00e-2$	$4.81e-3$	$5.51e-3$	$6.17e-3$	$9.10e-3$	$4.77e-2$	$1.02e-2$	$4.33e-3$
max	$4.03e-2$	$1.464e-1$	$5.03e-3$	$1.08e-1$	$2.36e-2$	$2.42e-2$	$1.31e-2$	$1.35e-2$	$9.37e-2$	$6.34e-2$	$1.51e-2$

Table 12: Summary statistics of the loss function components along the simulation path for the optimal solution of the stochastic model with pseudo-states.

Appendix C Leave-one-out error with Gaussian processes

The selection of the number of sample points n contained in the training set $\mathcal{D}$ is a trade-off between accuracy and efficiency: our design philosophy is to minimize n but still guarantee the accuracy of the surrogate model predictions based GP in a computationally affordable way.

One common choice in the UQ literature to strike a balance between these two opposing factors, although primarily discussed with polynomial chaos expansions (see, e.g., Blatman and Sudret (2010), Le Gratiet et al. (2017), Harenberg et al. (2019)), is to use the *leave-one-out* (LOO) error estimator. Recall that, as in Eq. (44), we have a computational model $\mathcal{M}(\cdot)$ that maps an input vector x_i to a scalar output y_i. We repeatedly evaluate Eq. (44) n times to obtain a training dataset $\mathcal{D} = \{x_i, y_i\}_{i=1}^n = [X, y]$. Then, we fit the GP interpolation of the original model $\mathcal{M}(\cdot)$, denoted as $\mathcal{M}_{\mathrm{GP}|X,y}(\cdot)$, as discussed in Section 4.1.2. To measure the LOO error, we first construct a GP surrogate model $\mathcal{M}_{\mathrm{GP}|X_{-i},y_{-i}}$ on experimental design points $X_{-i} \equiv X \setminus x_i = \{x_1, \cdots, x_{i-1}, x_{i+1}, \cdots, x_n\}$, and estimate the error Δ_i on the excluded point x_i between

the outcome from the true model and the prediction from the GP model, that is,

$$\Delta_i \equiv \mathcal{M}(x_i) - \mathcal{M}_{\mathrm{GP}|X_{-i},y_{-i}}(x_i) \tag{121}$$

Next, we compute the sum of Δ_i over i and define the LOO error, that is,

$$\epsilon_{\mathrm{LOO}}^{\mathrm{GP}} \equiv \frac{1}{n}\sum_{i=1}^{n}\Delta_i^2 = \frac{1}{N}\sum_{i=1}^{n}\left(\mathcal{M}(x_i) - \mathcal{M}_{\mathrm{GP}|X_{-i},y_{-i}}(x_i)\right)^2 . \tag{122}$$

In our numerical applications below, we choose the size of the training set n for the GP surrogate such that we achieve $\epsilon_{\mathrm{LOO}}^{\mathrm{GP}} \leq 10^{-2}$, which guarantees the required high accuracy of the GP surrogate for our QoIs, obtained at moderate computational costs. If a given initial n is insufficient, we systematically increase the size of the training set, e.g., by applying Bayesian active learning (see, e.g., Renner and Scheidegger (2018), and references therein).

References

Ackerman, F., E. A. Stanton, and R. Bueno (2010): "Fat Tails, Exponents, Extreme Uncertainty: Simulating Catastrophe in DICE," *Ecological Economics*, 69, 1657–1665. [5, 6]

Allen, M. R. and D. J. Frame (2007): "Call Off the Quest," *Science*, 318, 582–583. [2]

Anderson, B., E. Borgonovo, M. Galeotti, and R. Roson (2014): "Uncertainty in Climate Change Modeling: Can Global Sensitivity Analysis Be of Help?" *Risk Analysis*, 34, 271–293. [3, 6]

Anthoff, D., R. S. J. Tol, and G. W. Yohe (2009): "Risk Aversion, Time Preference, and the Social Cost of Carbon," *Environmental Research Letters*, 4, 024002. [5]

Azinovic, M., L. Gaegauf, and S. Scheidegger (2022): "Deep Equilibrium Nets," *International Economic Review*, n/a. [3, 7, 16, 44]

Barnett, M. (2023): "Climate change and uncertainty: An asset pricing perspective," *Management Science*. [5]

Barnett, M., W. Brock, and L. P. Hansen (2020): "Pricing Uncertainty Induced by Climate Change," *The Review of Financial Studies*, 33, 1024–1066. [6]

Bellman, R. E. (1961): *Adaptive Control Processes: A Guided Tour*, Princeton University Press. [3, 7]

Bergstra, J. S., R. Bardenet, Y. Bengio, and B. Kégl (2011): "Algorithms for Hyper-Parameter Optimization," in *Advances in neural information processing systems*, 2546–2554. [17]

Blatman, G. and B. Sudret (2010): "An Adaptive Algorithm to Build up Sparse Polynomial Chaos Expansions for Stochastic Finite Element Analysis," *Probabilistic Engineering Mechanics*, 25, 183–197. [50]

Brumm, J. and S. Scheidegger (2017): "Using Adaptive Sparse Grids to Solve High-Dimensional Dynamic Models," *Econometrica*, 85, 1575–1612. [1]

Butler, M. P., P. M. Reed, K. Fisher-Vanden, K. Keller, and T. Wagener (2014): "Identifying Parametric Controls and Dependencies in Integrated Assessment Models Using Global Sensitivity Analysis," *Environmental Modelling & Software*, 59, 10–29. [3, 6]

Cai, Y. and K. L. Judd (2014): "Advances in numerical dynamic programming and new applications," *Handbook of computational economics*, 3. [7]

Cai, Y., K. L. Judd, T. M. Lenton, T. S. Lontzek, and D. Narita (2015): "Environmental Tipping Points Significantly Affect the Cost-Benefit Assessment of Climate Policies," *Proceedings of the National Academy of Sciences of the United States of America*, 112, 4606–4611. [5]

Cai, Y., T. M. Lenton, and T. S. Lontzek (2016): "Risk of Multiple Interacting Tipping Points Should Encourage Rapid CO2 Emission Reduction," *Nature Climate Change*, 6, 520–525. [5]

Cai, Y. and T. S. Lontzek (2019): "The Social Cost of Carbon with Economic and Climate Risks," *Journal of Political Economy*, 127, 2684–2734. [2, 3, 5, 7, 8, 10, 21, 30, 33]

Chen, H., A. Didisheim, and S. Scheidegger (2021): "Deep Structural Estimation : With an Application to Option Pricing," Tech. rep. [3, 6]

Constantine, P. G. (2015): *Active Subspaces*, Philadelphia, PA: Society for Industrial and Applied Mathematics. [7]

Crost, B. and C. P. Traeger (2013): "Optimal Climate Policy: Uncertainty versus Monte Carlo," *Economics Letters*, 120, 552–558. [4, 6, 8]

——— (2014): "Optimal CO2 Mitigation under Damage Risk Valuation," *Nature Climate Change*, 4, 631–636. [4]

DeGroot, M. H. (1970): *Optimal Statistical Decisions*, Wiley. [14]

Duarte, V. (2018): "Machine Learning for Continuous-Time Economics," SSRN Scholarly Paper ID 3012602, Social Science Research Network, Rochester, NY. [7]

Ebrahimi Kahou, M., J. Fernández-Villaverde, J. Perla, and A. Sood (2021): "Exploiting Symmetry in High-Dimensional Dynamic Programming," Working Paper 28981, National Bureau of Economic Research. [7]

Eftekhari, A. and S. Scheidegger (2022): "High-Dimensional Dynamic Stochastic Model Representation," *SIAM Journal on Scientific Computing*, 44, C210–C236. [23]

Eftekhari, A., S. Scheidegger, and O. Schenk (2017): "Parallelized Dimensional Decomposition for Large-Scale Dynamic Stochastic Economic Models," in *Proceedings of the Platform for Advanced Scientific Computing Conference*, New York, NY, USA: ACM, PASC '17, 9:1–9:11. [23]

Epstein, L. G. and S. E. Zin (1989): "Substitution, Risk Aversion, and the Temporal Behavior of Consumption and Asset Returns: A Theoretical Framework," *Econometrica*, 57, 937. [2, 8]

Fernández-Villaverde, J., G. Nuño, G. Sorg-Langhans, and M. Vogler (2020): "Solving High-Dimensional Dynamic Programming Problems Using Deep Learning," Tech. rep. [7]

Fitzpatrick, L. G. and D. L. Kelly (2017): "Probabilistic Stabilization Targets," *Journal of the Association of Environmental and Resource Economists*, 4, 611–657. [5, 13]

Folini, D., A. Friedl, F. Kubler, and S. Scheidegger (2023): "The climate in climate economics," *Available at SSRN 3885021*. [2, 7, 8, 11, 12, 16, 30, 41]

Gillingham, K., W. Nordhaus, D. Anthoff, G. Blanford, V. Bosetti, P. Christensen, H. McJeon, and J. Reilly (2018): "Modeling Uncertainty in Integrated Assessment of Climate Change: A Multimodel Comparison," *Journal of the Association of Environmental and Resource Economists*, 5, 791–826. [5]

Glorot, X. and Y. Bengio (2010): "Understanding the difficulty of training deep feedforward neural networks," in *Proceedings of the Thirteenth International Conference on Artificial Intelligence and Statistics*, ed. by Y. W. Teh and M. Titterington, Chia Laguna Resort, Sardinia, Italy: PMLR, vol. 9 of *Proceedings of Machine Learning Research*, 249–256. [17]

Golosov, M., J. Hassler, P. Krusell, and A. Tsyvinski (2014): "Optimal Taxes on Fossil Fuel in General Equilibrium," *Econometrica*, 82, 41–88. [4]

Goodfellow, I., Y. Bengio, and A. Courville (2016): *Deep Learning*, MIT Press, `http://www.deeplearningbook.org`. [17]

Harenberg, D., S. Marelli, B. Sudret, and V. Winschel (2019): "Uncertainty Quantification and Global Sensitivity Analysis for Economic Models," *Quantitative Economics*, 10, 1–41. [3, 6, 22, 24, 25, 29, 50]

Hassler, J., P. Krusell, and A. A. Smith (2016): "Chapter 24 - Environmental Macroeconomics," Elsevier, vol. 2, 1893–2008. [4]

Hornik, K., M. Stinchcombe, and H. White (1989): "Multilayer Feedforward Networks are Universal Approximators," *Neural Networks*, 2, 359 – 366. [17]

Hwang, I. C., F. Reynès, and R. S. Tol (2017): "The Effect of Learning on Climate Policy under Fat-Tailed Risk," *Resource and Energy Economics*, 48, 1–18. [5, 13, 32]

Iooss, B. and C. Prieur (2019): "Shapley Effects for Sensitivity Analysis with Correlated Inputs: Comparisons with Sobol' Indices, Numerical Estimation and Applications," *International Journal for Uncertainty Quantification*, 9. [6, 26]

Jaynes, E. T. (1957): "Information Theory and Statistical Mechanics. II," *Physical review*, 108, 171–190. [23]

——— (1982): "On The Rationale of Maximum-Entropy Methods," *Proceedings of the IEEE*, 70, 939 – 952, cited by: 1118. [23]

Jensen, S. and C. Traeger (2013): "Optimally climate sensitive policy: A comprehensive evaluation of uncertainty & learning," *Department of Agricultural and Resource Economics, UC Berkeley*. [5, 32]

Jensen, S. and C. P. Traeger (2014): "Optimal Climate Change Mitigation under Long-Term Growth Uncertainty: Stochastic Integrated Assessment and Analytic Findings," *European Economic Review*, 69, 104–125. [2, 5, 30, 33]

Kelly, D. L. and C. D. Kolstad (1999): "Bayesian Learning, Growth, and Pollution," *Journal of Economic Dynamics and Control*, 23, 491–518. [5, 13]

Kelly, D. L. and Z. Tan (2015): "Learning and Climate Feedbacks: Optimal Climate Insurance and Fat Tails," *Journal of Environmental Economics and Management*, 72, 98–122. [5, 13, 14, 32]

Kingma, D. P. and J. Ba (2014): "Adam: A method for stochastic optimization," *arXiv preprint arXiv:1412.6980*. [19]

Knutti, R., M. A. A. Rugenstein, and G. C. Hegerl (2017): "Beyond Equilibrium Climate Sensitivity," *Nature Geoscience*, 10, 727–736. [2, 5, 12]

Kotlikoff, L., F. Kubler, A. Polbin, and S. Scheidegger (2021): "Pareto-improving carbon-risk taxation," *Economic Policy*, 36, 551–589. [2, 8, 10]

Kubler, F. and S. Scheidegger (2021): "Uniformly Self-Justified Equilibria," *Available at SSRN 3995209*. [7]

Le Gratiet, L., S. Marelli, and B. Sudret (2017): "Metamodel-Based Sensitivity Analysis: Polynomial Chaos Expansions and Gaussian Processes," in *Handbook of Uncertainty Quantification*, ed. by R. Ghanem, D. Higdon, and H. Owhadi, Cham: Springer International Publishing, 1289–1325. [50]

Leach, A. J. (2007): "The Climate Change Learning Curve," *Journal of Economic Dynamics and Control*, 31, 1728–1752. [5, 13]

Lemoine, D. and C. Traeger (2014): "Watch Your Step: Optimal Policy in a Tipping Climate," *American Economic Journal: Economic Policy*, 6, 137–166. [5]

Lemoine, D. and C. P. Traeger (2016): "Economics of Tipping the Climate Dominoes," *Nature Climate Change*, 6, 514–519. [5]

Lenton, T. M., H. Held, E. Kriegler, J. W. Hall, W. Lucht, S. Rahmstorf, and H. J. Schellnhuber (2008): "Tipping elements in the Earth's climate system," *Proceedings of the national Academy of Sciences*, 105, 1786–1793. [2, 6, 10]

Lontzek, T. S., Y. Cai, K. L. Judd, and T. M. Lenton (2015): "Stochastic Integrated Assessment of Climate Tipping Points Indicates the Need for Strict Climate Policy," *Nature Climate Change*, 5, 441–444. [5]

Lontzek, T. S. and D. Narita (2011): "Risk-Averse Mitigation Decisions in an Unpredictable Climate System," *The Scandinavian Journal of Economics*, 113, 937–958. [5]

Lontzek, T. S., D. Narita, and O. Wilms (2016): "Stochastic Integrated Assessment of Ecosystem Tipping Risk," *Environmental and Resource Economics*, 65, 573–598. [5]

Ma, X. and N. Zabaras (2010): "An Adaptive High-Dimensional Stochastic Model Representation Technique for the Solution of Stochastic Partial Differential Equations," *J. Comput. Phys.*, 229, 3884–3915. [23]

Maliar, L., S. Maliar, and P. Winant (2021): "Deep Learning for Solving Dynamic Economic Models," *Journal of Monetary Economics*, 122, 76–101. [7, 47]

Marrel, A., B. Iooss, B. Laurent, and O. Roustant (2009): "Calculations of Sobol Indices for the Gaussian Process Metamodel," *Reliability Engineering & System Safety*, 94, 742–751. [24, 25]

Miftakhova, A. (2021): "Global sensitivity analysis for optimal climate policies: Finding what truly matters," *Economic Modelling*, 105, 105653. [3, 6]

Murphy, K. P. (2012): *Machine Learning: A Probabilistic Perspective*, The MIT Press. [20]

——— (2022): *Probabilistic Machine Learning: Advanced Topics*, MIT Press. [20]

Nordhaus, W. D. (2008): *A Question of Balance: Weighing the Options on Global Warming Policies*, Yale University Press. [4, 6]

——— (2017): "Revisiting the Social Cost of Carbon," *Proceedings of the National Academy of Sciences*, 114, 1518 LP – 1523. [2, 8, 9, 10, 11, 21, 30]

——— (2018): "Projections and Uncertainties about Climate Change in an Era of Minimal Climate Policies," *American Economic Journal: Economic Policy*, 10, 333–360. [5]

Oakley, J. E. and A. O'Hagan (2004): "Probabilistic Sensitivity Analysis of Complex Models: A Bayesian Approach," *Journal of the Royal Statistical Society: Series B (Statistical Methodology)*, 66, 751–769. [24]

Owen, A. B. (2014): "Sobol' Indices and Shapley Value," *SIAM/ASA Journal on Uncertainty Quantification*, 2, 245–251. [3, 6, 25, 26]

Pindyck, R. S. (2013): "Climate Change Policy: What Do the Models Tell Us?" *Journal of Economic Literature*, 51, 860–872. [1]

Rasmussen, C. E. and C. K. I. Williams (2005): *Gaussian Processes for Machine Learning (Adaptive Computation and Machine Learning)*, The MIT Press. [19, 20]

Renner, P. and S. Scheidegger (2018): "Machine learning for dynamic incentive problems," *Available at SSRN 3462011*, working paper. [4, 7, 21, 51]

Roe, G. H. and M. B. Baker (2007): "Why Is Climate Sensitivity So Unpredictable?" *Science*, 318, 629–632. [2, 12, 13, 30]

Saltelli, A. and B. D'Hombres (2010): "Sensitivity Analysis Didn't Help. A Practitioner's Critique of the Stern Review," *Global Environmental Change*, 20, 298–302. [6]

Saltelli, A., M. Ratto, T. Andres, F. Campolongo, J. Cariboni, D. Gatelli, M. Saisana, and S. Tarantola (2007): *Global Sensitivity Analysis. The Primer*, Chichester, UK: John Wiley & Sons, Ltd. [2, 22, 23, 25]

Scheidegger, S. and I. Bilionis (2019): "Machine Learning for High-Dimensional Dynamic Stochastic Economies," *Journal of Computational Science*, 33, 68–82. [6, 16]

Shapley, L. S. (1953): "A Value for N-Person Games," in *Contributions to the Theory of Games (AM-28), Volume II*, ed. by H. W. Kuhn and A. W. Tucker, Princeton: Princeton University Press, 307–318. [25]

Smith, R. C. (2014): *Uncertainty Quantification: Theory, Implementation, and Applications*, Society for Industrial and Applied Mathematics. [6]

Sobol, I. M. (2001): "Global Sensitivity Indices for Nonlinear Mathematical Models and Their Monte Carlo Estimates," *Mathematics and Computers in Simulation*, 55, 271–280. [23, 24]

Song, E., B. L. Nelson, and J. Staum (2016): "Shapley Effects for Global Sensitivity Analysis: Theory and Computation," *SIAM/ASA Journal on Uncertainty Quantification*, 4, 1060–1083. [3, 6, 25, 26]

Stern, N. (2008): "The Economics of Climate Change," *American Economic Review*, 98, 1–37. [30]

Sudret, B. (2008): "Global Sensitivity Analysis Using Polynomial Chaos Expansions," *Reliability Engineering & System Safety*, 93, 964–979. [22, 23, 24]

Sun, Y., D. W. Apley, and J. Staum (2011): "Efficient Nested Simulation for Estimating the Variance of a Conditional Expectation," *Operations Research*, 59, 998–1007. [26]

Traeger, C. P. (2014): "A 4-Stated DICE: Quantitatively Addressing Uncertainty Effects in Climate Change," *Environmental and Resource Economics*, 59, 1–37. [4, 21, 42]

——— (2021): "ACE – Analytic Climate Economy," SSRN Scholarly Paper ID 3832722, Social Science Research Network, Rochester, NY. [4]

van der Ploeg, F. (2021): "Carbon pricing under uncertainty," *International Tax and Public Finance*, 28, 1122–1142. [5]

Villa, A. T. and V. Valaitis (2019): "Machine Learning Projection Methods for Macro-Finance Models," Tech. rep. [7]

Webster, M., L. Jakobovits, and J. Norton (2008): "Learning about Climate Change and Implications for Near-Term Policy," *Climatic Change*, 89, 67–85. [13]

Weil, P. (1989): "The Equity Premium Puzzle and the Risk-Free Rate Puzzle," *Journal of Monetary Economics*, 24, 401–421. [8]

Weitzman, M. L. (2012): "GHG Targets as Insurance Against Catastrophic Climate Damages," *Journal of Public Economic Theory*, 14, 221–244. [2, 6, 10, 30]

Winter, E. (2002): "The Shapley Value," in *Handbook of Game Theory with Economic Applications*, Elsevier, vol. 3, 2025–2054. [25]

Younes, A., T. A. Mara, N. Fajraoui, F. Lehmann, B. Belfort, and H. Beydoun (2013): "Use of Global Sensitivity Analysis to Help Assess Unsaturated Soil Hydraulic Parameters," *Vadose Zone Journal*, 12. [25]

Zaliapin, I. and M. Ghil (2010): "Another Look at Climate Sensitivity," *Nonlinear Processes in Geophysics*, 17, 113–122. [2, 12]

Zhao, Y., A. Basu, T. S. Lontzek, and K. Schmedders (0): "The Social Cost of Carbon When We Wish for Full-Path Robustness," *Management Science*, 0, null. [6]